

# NumCalc: An open source BEM code for solving acoustic scattering problems

W. Kreuzer<sup>a,\*</sup>, K. Pollack<sup>a</sup>, F. Brinkmann<sup>b</sup>, P. Majdak<sup>a</sup>

<sup>a</sup>*Austrian Academy of Sciences, Acoustics Research Institute, Wohlebengasse 12-14, 1040, Vienna, Austria*

<sup>b</sup>*Audio Communication Group, Technical University of Berlin, Straße des 17. Juni 135, 10623, Berlin, Germany*

---

## Abstract

The calculation of the acoustic field in or around objects is an important task in acoustic engineering. To numerically solve this task, the boundary element method (BEM) is a commonly used method especially for infinite domains. The open source tool Mesh2HRTF and its BEM core NumCalc provide users with a collection of free software for acoustic simulations without the need of having an in-depth knowledge into numerical methods. However, we feel that users should have a basic understanding with respect to the methods behind the software they are using. We are convinced that this basic understanding helps in avoiding common mistakes and also helps to understand the requirements to use the software. To provide this background is the first motivation for this paper. A second motivation for this paper is to demonstrate the accuracy of NumCalc when solving benchmark problems. Thus, users can get an idea about the accuracy they can expect when using NumCalc as well as the memory and CPU requirements of NumCalc. A third motivation for this paper is to give users detailed information about some parts of the actual implementation that are usually not mentioned in literature, e.g., the specific version of the fast multipole method and its clustering process or how to use frequency-dependent admittance boundary conditions.

*Keywords:* BEM, Software, Fast Multipole Method

---

## 1. Introduction

The boundary element method (BEM, [1, 2]) has a long tradition for numerically solving the Helmholtz equation in 3D that models acoustic wave propagation in the frequency domain. Compared to other methods such as the finite element method [3] (FEM), the BEM has the advantage that only the surface of the scattering object needs to be considered and that for external problems the decay of the acoustic wave towards infinity is already included in the formulation. This renders the BEM an attractive tool for calculating sound-wave propagation. However, the BEM has the drawback that the generated linear system of equations

---

\*Corresponding author.

*Email addresses:* wolfgang.kreuzer@oeaw.ac.at (W. Kreuzer), katharina.pollack@oeaw.ac.at (K. Pollack), fabian.brinkmann@tu-berlin.de (F. Brinkmann), piotr.majdak@oeaw.ac.at (P. Majdak)

has a densely populated system matrix. To tackle this problem, the combination of BEM and fast methods for matrix-vector multiplications such as the fast multipole method (FMM, [4, 5, 6]) or  $\mathcal{H}$ -matrices [7] were introduced. Eventually, BEM-based acoustic modeling became an increasingly popular tool for engineers, as illustrated by various software packages such as COMSOL [8], FastBEMAcoustics [9], AcouSTO [10], BEMpp [11], or OpenBEM [12].

NumCalc [13] is an open-source program written in C++ for solving the Helmholtz equation in 3D. It is based on collocation with constant elements in combination with an implementation of the FMM to speed up matrix-vector multiplications. NumCalc is distributed in the framework of Mesh2HRTF [14, 15, 16], which is aimed at the numerical calculation and post processing of head-related transfer functions (HRTFs, [17]). HRTFs describe the direction-dependent filtering of a sound source due to the listener’s body especially by the head and ears and are usually acoustically measured [18, 19].

The basic idea for Mesh2HRTF is to provide an open-source code that is easy-to-use for researchers without the need for an extensive background in mathematics or physics, specifically targeting users not familiar with BEM. To this end, Mesh2HRTF contains an add-on for the open-source program Blender [20] and automatically generates the input for NumCalc. The accompanying project websites [15, 21] provide tutorials for creating a valid description of the geometry of the scattering object and its materials. Despite the encapsulation of the BEM calculations from the typical Mesh2HRTF user, some rules are required for correct calculations and their compliance cannot be ensured by the Mesh2HRTF interface. Hence, the main goal of the article is to explain such rules, provide insights to what can happen if they are violated, and how to avoid common mistakes. To this end, throughout the article, we point out the most important rules as hints:

*“Hint 0: Look out for these lines.”*

Although part of the Mesh2HRTF-project, NumCalc is *not restricted* to calculations of HRTFs only. The input to NumCalc is a general definition of surface meshes, based on triangular or plane quadrilateral elements, arbitrary admittance boundary conditions can be assigned to each element, and external sound sources can be modelled as plane waves or as point sources (see [Appendix A](#) and [Appendix B](#)). NumCalc can be used to solve general wave scattering problems in 3D using the BEM.

This article describes the general features of NumCalc in detail for the first time in one manuscript. It provides all necessary information for users to responsibly use NumCalc for their problem at hand, including some benchmark tests to measure its accuracy and needs with respect to memory consumption. Besides specific aspects of the implementation of the BEM, such as the quasi-singular quadrature or the possibility to define frequency-dependent boundary conditions, we for the first time give a detailed description on the specific flavour and implementation of the FMM. This includes a description, how the clusters are generated and how one can derive all matrices necessary for the fast multipole method. Compared to other standard

implementations of the FMM the root level already consists of multiple clusters and the local element-to-cluster expansion matrices on *all* levels of a multilevel FMM are stored explicitly, which reduces computing time. As the root level already consists of many clusters, the truncation length of the multipole expansion and in turn the memory necessary to use NumCalc can be kept relatively low. Finally, we provide numerical experiments that illustrate the accuracy of NumCalc, show how the mesh is clustered in the default setting and discuss the memory required for the FMM algorithm based on the clustering.

This article is structured as follows: In Sec. 2 we describe the general aspects of the BEM and the way they are implemented in NumCalc. In Sec. 3, we provide specific details of the implementation of the quadrature and clustering in NumCalc. In Sec. 4, we focus on the critical components of the implementation and their effect on accuracy and computational effort. Sec. 5 presents three benchmark problems solved with NumCalc to demonstrate the achievable accuracy and the need of computing power. Finally, we summarize and discuss the results in Sec. 6. To keep the paper self contained, Appendix A provides the definition of a mesh to describe the geometry of the scatterer, Appendix B provides examples for NumCalc input files including how to define frequency-dependent admittance boundary conditions, Appendix C gives a description of possible command line parameters and Appendix D lists the different output files generated by NumCalc.

## 2. BEM and its Implementation in NumCalc

In a nutshell, NumCalc implements the direct BEM using collocation with constant elements in combination with the Burton-Miller method. Per default, an iterative solver is used to solve the system of equations, and the matrix-vector multiplications are sped up using the FMM. To keep the paper self-contained, we start with a brief introduction to collocation BEM, explaining the requirements for the meshes used for the BEM.

Figure 1 shows a typical situation of an (exterior) acoustics wave scattering problem. An incoming point source outside the scatterer  $\Omega$  is positioned at a point  $\mathbf{x}_{\text{inc}}$ . The acoustic wave produced by this source is scattered and reflected at the surface  $\Gamma$  of the scatterer. With the BEM, the acoustic field on the surface  $\Gamma$  at nodes  $\mathbf{x}_\Gamma$  as well as on exterior nodes  $\mathbf{x}_o$  outside  $\Gamma$  is determined. The main goal of NumCalc is to derive the acoustic pressure  $p$  and the particle velocity  $v$  at both the points on the surface  $\Gamma$  of the scatterer  $\Omega$  and the evaluation points  $\mathbf{x}_o$  in the free-field  $\mathbb{R}^3 \setminus \Gamma$ . To this end, NumCalc solves the Helmholtz equation describing the free-field sound propagation in the frequency domain:

$$\nabla^2 p(\mathbf{x}, \omega) + k^2 p(\mathbf{x}, \omega) = p_0(\mathbf{x}, \mathbf{x}_{\text{inc}}, \omega), \quad \mathbf{x} \in \mathbb{R}^3 \setminus \Gamma, \quad (1)$$

with  $p$  being the sound pressure,  $k = \frac{\omega}{c} = \frac{2\pi f}{c}$  the wavenumber for a given frequency  $f$  and speed of sound  $c$ , and  $p_0$  being an external sound source located at  $\mathbf{x}_{\text{inc}}$ .

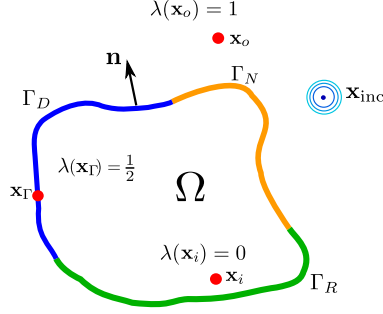


Figure 1: Scheme of an exterior problem with scatterer  $\Omega$  with boundary  $\Gamma = \Gamma_D \cup \Gamma_N \cup \Gamma_R$ , a point-source at  $\mathbf{x}_{\text{inc}}$ , interior point  $\mathbf{x}_i$ , exterior point  $\mathbf{x}_o$  and a node on the boundary  $\mathbf{x}_\Gamma$ .

To model the acoustic properties of the surface  $\Gamma$ , a boundary condition (bc) is defined for each point on the surface  $\Gamma$ . Thus, either the sound pressure  $p$  (Dirichlet bc), the particle velocity  $v$  (Neumann bc) or a combination of both (Robin bc) are known:

$$\begin{aligned} p(\mathbf{x}) &= f(\mathbf{x}) & \mathbf{x} \in \Gamma_D, \\ v(\mathbf{x}) &= g(\mathbf{x}) & \mathbf{x} \in \Gamma_N, \\ \alpha p(\mathbf{x}) + \beta v(\mathbf{x}) &= h(\mathbf{x}) & \mathbf{x} \in \Gamma_R, \end{aligned}$$

for given functions  $f, g, h$ , and constants  $\alpha, \beta$ .

### 2.1. The boundary integral equation (BIE)

The acoustic field at a point  $\mathbf{x}$  can be represented by the sound pressure  $p(\mathbf{x})$  and the particle velocity  $v(\mathbf{x})$  at this point, which in the frequency domain can both be derived from the velocity potential  $\phi(\mathbf{x})$  using

$$p(\mathbf{x}) = -i\omega\rho\phi(\mathbf{x}), \quad v(\mathbf{x}) = \frac{\partial\phi}{\partial\mathbf{n}}(\mathbf{x}) = \nabla\phi(\mathbf{x}) \cdot \mathbf{n}(\mathbf{x}), \quad (2)$$

where  $\omega = 2\pi f$  is the angular frequency, and  $\rho$  denotes the density of the medium. If  $\mathbf{x} \in \Gamma$  the particle velocity is defined using the normal vector  $\mathbf{n}$  to the surface pointing to the outside. If the point  $\mathbf{x}$  lies in the free field it can be any arbitrary vector with  $\|\mathbf{n}\| = 1$ .

In order to solve the Helmholtz equation, the partial differential equation needs to be transformed into an integral equation. In general, there are two possibilities for this transformation, direct and indirect BEM (cf. [2]). In NumCalc, the direct formulation based on Green's representation formula is used:

$$\lambda(\mathbf{x})\phi(\mathbf{x}) - \tau \int_{\Gamma} H(\mathbf{x}, \mathbf{y})\phi(\mathbf{y})d\mathbf{y} + \tau \int_{\Gamma} G(\mathbf{x}, \mathbf{y})v(\mathbf{y})d\mathbf{y} = \phi_{\text{inc}}(\mathbf{x}), \quad (3)$$

where  $G(\mathbf{x}, \mathbf{y}) = \frac{e^{ik|\mathbf{x}-\mathbf{y}|}}{4\pi|\mathbf{x}-\mathbf{y}|}$  is the Green's function for the free-field Helmholtz equation,  $H(\mathbf{x}, \mathbf{y}) = \frac{\partial G}{\partial\mathbf{n}_y}(\mathbf{x}, \mathbf{y}) = \nabla G(\mathbf{x}, \mathbf{y}) \cdot \mathbf{n}(\mathbf{y}) = G(\mathbf{x}, \mathbf{y}) \left( ik - \frac{1}{r} \right) \frac{\mathbf{x}-\mathbf{y}}{r} \cdot \mathbf{n}(\mathbf{y})$ ,  $r = \|\mathbf{x} - \mathbf{y}\|$ , and  $\phi_{\text{inc}}$  is the velocity potential caused by

an external sound source, e.g., a point source positioned at  $\mathbf{x}_{\text{inc}}$ . The parameter  $\tau$  indicates the problem setting. If  $\tau = -1$ , the acoustic field *inside* the object is of interest, in this case, we speak of an “interior” problem. If  $\tau = 1$  the acoustic field outside the object is of interest, in that case, we have an “exterior” problem.

The integrands in Eq. (3) depend on the derivative with respect to the normal vector  $\mathbf{n}_y := \mathbf{n}(\mathbf{y})$ . Normal vectors pointing in the different directions cause a sign change, essentially mixing up the roles of interior and exterior problems. As a consequence, Eq. (3) may produce incorrect results. To avoid this, it is essential that  $\mathbf{n}_y$  points away from the scatterer, however, NumCalc does not check this. This check is left to the user:

*“Hint 1: Check if your normal vectors point away from the scatterer.”*

Note, that if the distance  $r = \|\mathbf{x} - \mathbf{y}\|$  between two points  $\mathbf{x}$  and  $\mathbf{y}$  becomes small,  $G$  and  $H$  behave like  $\frac{1}{r}$ . Thus, special methods are needed to numerically calculate the integrals over  $\Gamma$ . We describe these methods in Sec. 3.1.

Note also, that Eq. (3) cannot be solved uniquely at resonance frequencies of the inner problem [22, 23]. For exterior problems, this can be handled using either CHIEF points [23] or the Burton-Miller method [22]. NumCalc implements the Burton-Miller method and the implementation is described in Sec. 2.5.

Finally, note that  $\lambda(\mathbf{x})$  depends on the position of the point  $\mathbf{x}$  (see also Fig. 1). If  $\mathbf{x}$  lies in the interior of the object  $\Omega$ ,  $\lambda(\mathbf{x}) = 0$ . If  $\mathbf{x}$  lies outside the object,  $\lambda(\mathbf{x}) = 1$ . If  $\mathbf{x}$  lies on a smooth part of the surface  $\lambda(\mathbf{x}) = \frac{1}{2}$ .

## 2.2. Discretization of the Geometry and Shapefunctions

To transform the BIE into a linear system of equations, the unknown solution of Eq. (3), i.e.,  $\phi(\mathbf{x})$  or  $v(\mathbf{x})$  on the surface (depending on the boundary condition at  $\mathbf{x}$ ), needs to be approximated by simple ansatz functions (= shape functions). To this end, the geometry of the scatterer’s surface is approximated by a mesh consisting of  $N$  elements  $\Gamma_j, j = 1, \dots, N$ . In NumCalc these elements can be triangular or *plane* quadrilateral, and on each of them, the BIE solution is assumed to be constant:

$$\phi(\mathbf{x}) = \begin{cases} \phi_j & \mathbf{x} \in \Gamma_j, \\ 0 & \text{otherwise.} \end{cases}$$

The number of elements  $N$  is a compromise between calculation time and numerical accuracy. The numerical accuracy is actually frequency dependent because the unknown solution with its oscillating parts needs to be represented accurately by the constant ansatz functions. As a rule of thumb, the mesh should contain six to eight elements per wavelength [24]. NumCalc does a check on that and displays a warning if the average size of the elements is too low, however, it will still do the calculations. This is because, in certain cases,

acceptable results can be achieved, when “irrelevant” parts of the mesh have a coarser discretization [25, 26]. The decision on the number of elements is within the responsibility of the user:

*“Hint 2: Check if your mesh contains 6-to-8 elements per wavelength in the relevant geometry regions.”*

Also, it is known, that for some problems, and that especially close to sharp edges and corners, a finer discretization than 6-to-8 elements per wavelength might be necessary [27], thus one should be aware, that the 6-to-8 elements per wavelength rule is just a rule of thumb.

The elements of the mesh are also used to calculate the integrals over the surface  $\Gamma$ . In NumCalc, integrals over  $\Gamma$  are replaced by sums of integrals over each element:

$$\int_{\Gamma} H(\mathbf{x}, \mathbf{y})\phi(\mathbf{y})d\mathbf{y} \approx \sum_{j=1}^N \int_{\Gamma_j} H(\mathbf{x}, \mathbf{y})\phi(\mathbf{y})d\mathbf{y} \approx \sum_{j=1}^N \int_{\Gamma_j} H(\mathbf{x}, \mathbf{y})d\mathbf{y}\phi_j. \quad (4)$$

As  $\Gamma_j$  represents a simple geometric element, the integrals over each element can be calculated relatively easily. By using the shape functions in combination with the boundary conditions, the unknown solution of Eq. (3) can be reduced to  $N$  unknowns (either  $\phi_j$  or  $v_j$ , depending on the given boundary condition).

### 2.3. Collocation

In order to derive a linear system of equations, NumCalc uses the collocation method, i.e., after the unknown solution is represented using the shape functions, Eq. (3) is evaluated at  $N$  collocation nodes  $\mathbf{x}_i$  for  $i = 1, \dots, N$ . For constant elements these nodes are, in general, the midpoints of each element  $\Gamma_i$  defined as the mean over the coordinates of the element’s vertices. Note, that because the collocation nodes are located inside the smooth plane element,  $\lambda(\mathbf{x}_i) = \frac{1}{2}$ , for  $i = 1, \dots, N$ , and Eq. (3) becomes

$$\frac{\phi_i}{2} - \tau \sum_{j=1}^N \left( \int_{\Gamma_j} H(\mathbf{x}_i, \mathbf{y})d\mathbf{y} \right) \phi_j + \tau \sum_{j=1}^N \left( \int_{\Gamma_j} G(\mathbf{x}_i, \mathbf{y})d\mathbf{y} \right) v_j = \phi_{\text{inc}}(\mathbf{x}_i), \quad (5)$$

where  $\phi_i = \phi(\mathbf{x}_i)$  and  $v_i = v(\mathbf{x}_i)$ ,  $i = 1, \dots, N$ , are the velocity potential and the particle velocity at the midpoint  $\mathbf{x}_i$  of each element, respectively. By defining the vectors

$$\boldsymbol{\phi} := (\phi_1, \dots, \phi_N)^\top, \quad \mathbf{v} := (v_1, \dots, v_N)^\top, \quad \boldsymbol{\phi}_{\text{inc}} = (\phi_{\text{inc}}(\mathbf{x}_1), \dots, \phi_{\text{inc}}(\mathbf{x}_N))^\top$$

and the matrices

$$\mathbf{H}_{ij} = \int_{\Gamma_j} H(\mathbf{x}_i, \mathbf{y})d\mathbf{y}, \quad \mathbf{G}_{ij} = \int_{\Gamma_j} G(\mathbf{x}_i, \mathbf{y})d\mathbf{y} \quad (6)$$

we obtain the discretized BIE in matrix-vector form:

$$\frac{\boldsymbol{\phi}}{2} - \tau \mathbf{H}\boldsymbol{\phi} + \tau \mathbf{G}\mathbf{v} = \boldsymbol{\phi}_{\text{inc}}, \quad (7)$$

which is a basis for further consideration to solve the Helmholtz equation numerically.

#### 2.4. Incoming Sound Sources

Incoming sound sources  $\phi_{\text{inc}}$  are the sources not positioned on the surface of the scatterer but located in the free field. NumCalc implements two types of incoming sound sources: Plane waves and point sources. A plane wave is defined by its strength  $S_0$  and its direction  $\mathbf{d}$ :

$$\phi_{\text{inc}}(\mathbf{x}) = S_0 e^{ik\mathbf{x}\cdot\mathbf{d}},$$

and a point source is defined by its strength  $S_0$  and its position  $\mathbf{x}^*$ :

$$\phi_{\text{inc}}(\mathbf{x}) = S_0 \frac{e^{ik\|\mathbf{x}-\mathbf{x}^*\|}}{4\pi\|\mathbf{x}-\mathbf{x}^*\|}, \quad (8)$$

with  $k$  being the wavenumber. From the definition of the point source it becomes clear, that if the source position  $\mathbf{x}^*$  is very close to the surface, the denominator in Eq. (8) will become zero, causing numerical problems. Thus,

*“Hint 3: Have at least the distance of one average edge length between an external sound source and the surface.”*

If sound sources very close to the surface or even on the surface are needed, a velocity boundary condition different from zero at the elements close to the source may be a better choice.

#### 2.5. The Burton-Miller Method

NumCalc implements the Burton-Miller approach to ensure a stable and unique solution of Eq. (7) for exterior problems at all frequencies. The final system of equations is derived by combining Eq. (3) and its derivative with respect to the normal vector at  $\mathbf{x}$

$$\lambda(\mathbf{x})v(\mathbf{x}) - \tau \int_{\Gamma} E(\mathbf{x}, \mathbf{y})\phi(\mathbf{y})d\mathbf{y} + \tau \int_{\Gamma} H'(\mathbf{x}, \mathbf{y})v(\mathbf{y})d\mathbf{y} = v_{\text{inc}}(\mathbf{x}), \quad (9)$$

where  $E(\mathbf{x}, \mathbf{y}) = \frac{\partial^2 G(\mathbf{x}, \mathbf{y})}{\partial \mathbf{n}_x \partial \mathbf{n}_y}$  and  $H'(\mathbf{x}, \mathbf{y}) = \frac{\partial G(\mathbf{x}, \mathbf{y})}{\partial \mathbf{n}_x}$ . The matrix-vector representation of Eq. (9) is then derived in a similar manner as that for Eq. (7).

The final system of equations to be solved reads then as

$$\frac{(\boldsymbol{\phi} - \gamma \mathbf{v})}{2} - \tau (\mathbf{H} - \gamma \mathbf{E}) \boldsymbol{\phi} + \tau (\mathbf{G} - \gamma \mathbf{H}') \mathbf{v} = \boldsymbol{\phi}_{\text{inc}} - \gamma \mathbf{v}_{\text{inc}}, \quad (10)$$

where

$$\mathbf{E}_{ij} = \int_{\Gamma_j} E(\mathbf{x}_i, \mathbf{y})d\mathbf{y}, \quad \mathbf{H}'_{ij} = \int_{\Gamma_j} H'(\mathbf{x}_i, \mathbf{y})d\mathbf{y}, \quad \mathbf{v}_{\text{inc}} = (v_{\text{inc}}(\mathbf{x}_1), \dots, v_{\text{inc}}(\mathbf{x}_N))^{\top}, \quad (11)$$

and  $\gamma := \frac{i}{k}$  is the coupling factor introduced by the Burton-Miller method [22, 28].

Because for each individual element, a boundary condition (pressure, velocity, or admittance) is given, either  $\phi_i$ ,  $v_i$ , or a relation between them is known. Thus, the final system of equations Eq. (10) has  $N$

unknowns and there are as many collocation nodes as unknowns, meaning that it can be solved by regular methods, e.g., either a direct solver [29] or an iterative solvers [30]. For most problems, the matrices in that system are, in general, densely populated and the number of unknowns can be large, thus, iterative solvers are the most common option. However, for large  $N$ , the cost of the matrix-vector multiplications needed by an iterative solver becomes too high. For those systems, the BEM can be coupled with methods for fast matrix-vector multiplications, e.g.  $\mathcal{H}$ -matrices [7] or the in NumCalc implemented FMM [4].

### 3. Specific Details on Deriving and Solving the System Equation

#### 3.1. Quadrature

In order to solve the BIE, the integrals in  $\mathbf{G}, \mathbf{H}, \mathbf{H}'$ , and  $\mathbf{E}$  defined in Eqs. (6) and (11) need to be calculated numerically. If the collocation node  $\mathbf{x}_i$  lies in the element for which the integral needs to be calculated, the integrand becomes singular because of the singularities of the Green's function and its derivatives. In this case, these integrals have to be calculated using special methods for the singular and the hypersingular integrals. For integrals over elements that do not contain the collocation node, we distinguish between elements that are close to the collocation node and elements far away which are solved by the quasi-singular quadrature and the regular quadrature, respectively.

##### 3.1.1. Singular Quadrature

For  $i = j$ , the integrands in Eq. (6) behave like  $\frac{1}{r}$  for  $r := \|\mathbf{x}_i - \mathbf{y}\| \rightarrow 0$ . In this case, NumCalc regularizes the integrals by using a quadrature method based on [31]. If the element  $\Gamma_i$  is triangular, it is subdivided into six triangles, where the collocation node  $\mathbf{x}_i$ , at which the singularity occurs, is a vertex of each of the sub-triangles. For a quadrilateral element, eight triangular sub-elements are created. Similar to [31], the integrals over each of these sub-triangles are transformed into integrals over the unit square which removes the singularity. After that transformation, the integral is computed using a Gauss quadrature with  $4 \times 4$  quadrature nodes.

For the singular quadrature with kernel  $\mathbf{H}(\mathbf{x}, \mathbf{y})$ , we can use the fact that, if  $\mathbf{x}$  and  $\mathbf{y}$  are in the same planar element,  $(\mathbf{x} - \mathbf{y})$  is orthogonal to  $\mathbf{n}_y$ . This yields  $H(\mathbf{x}, \mathbf{y}) = \nabla_y G(\mathbf{x}, \mathbf{y}) \cdot \mathbf{n}_y = \frac{dG}{dr} \frac{\partial r}{\partial \mathbf{y}} \cdot \mathbf{n}_y = -\frac{dG}{dr} \frac{\mathbf{x} - \mathbf{y}}{r} \cdot \mathbf{n}_y = 0$ . The same argument can be used for the contributions with respect to  $\mathbf{H}'$ .

##### 3.1.2. Hypersingular Quadrature

To calculate the integrals involving the hypersingular kernel  $E(\mathbf{x}, \mathbf{y})$ , the integral involving the hypersingular kernel is split into integrals over the edges of the element and the element itself [32]:

$$\mathbf{E}_{ii} = \int_{\Gamma_i} E(\mathbf{x}_i, \mathbf{y}) d\mathbf{y} = \sum_{\ell, m, n=1}^3 \mathbf{n}_\ell \epsilon_{\ell mn} \oint_{\partial \Gamma_i} \frac{\partial G}{\partial y_m}(\mathbf{x}_i, \mathbf{y}) dy_n + k^2 \int_{\Gamma_i} G(\mathbf{x}_i, \mathbf{y}) d\mathbf{y}, \quad (12)$$

where  $\epsilon_{\ell mn}$  is the Levi-Civita-symbol

$$\epsilon_{\ell mn} = \begin{cases} 1 & \text{if } (\ell, m, n) \in \{(1, 2, 3), (2, 3, 1), (3, 1, 2)\}, \\ -1 & \text{if } (\ell, m, n) \in \{(3, 2, 1), (1, 3, 2), (2, 1, 3)\}, \\ 0 & \text{if } \ell = m, \ell = n, m = n, \end{cases}$$

and  $\mathbf{y} = (y_1, y_2, y_3)$  is a point on the element  $\Gamma_i$ ,  $\mathbf{n}_\ell$  is the  $\ell$ -th component of the normal vector  $\mathbf{n}$ , and  $\partial\Gamma_i$  denotes the edges of the element. For the integral over the edges  $\partial\Gamma_i$ , each edge is subdivided into 4 equally sized parts, and on each part, a Gaussian quadrature with 3 nodes is used. The integral over the element  $\Gamma_i$  is calculated using the singular quadrature described in Sec. 3.1.1.

### 3.1.3. Quasi-singular Quadrature

NumCalc calculates the quasi-singular integrals in two steps: First, if the relative distance  $\tilde{r} = \frac{\|\mathbf{x}_i - \mathbf{x}_j\|}{\sqrt{A_j}}$  of the midpoint  $\mathbf{x}_j$  of  $\Gamma_j$  and the collocation node  $\mathbf{x}_i$  is smaller than 1.3, the element is subdivided into four subelements, with  $A_j$  being the area of the subelement  $\Gamma_j$ . This procedure is repeated for all subelements until the condition is fulfilled. As result, the distance between the collocation node and the subelement will be larger than the edge length of that subelements. This procedure is visualized in Fig. 2. Note, that this way, the quadrature grid gets finer close to the collocation node. The factor 1.3 was heuristically chosen as a good compromise between accuracy and efficiency. Once the subelements are constructed, the integrals over them can be solved using the regular quadrature.

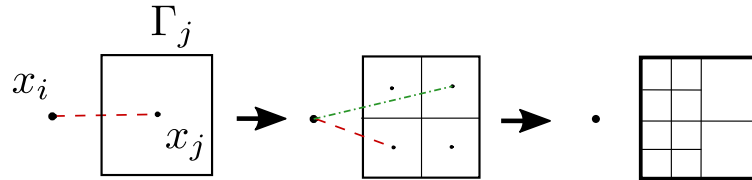


Figure 2: Example of two levels of element subdivisions in the quasi-singular quadrature and a quadrilateral element. The dashed (red) line shows the distance between the two nodes, which is too small compared to the average edge length, thus the element needs to be divided. The dashed-dotted (green) line shows the distance which is sufficiently large such that no further division is necessary.

Note that the distance between the element midpoints is just an approximation for the actually required smallest distance between the collocation node and *all* the points of an element. NumCalc uses the distance between the element midpoints because calculations can be done efficiently and it works well for regular elements. Thus,

*“Hint 4: Keep the elements as regular as possible.”*

If an element is not regular, e.g., stretched in one direction, the approach of iterative subdivisions may fail.

### 3.1.4. Regular Quadrature

If the element and the collocation node are sufficiently far apart from each other, NumCalc determines the order of the Gauss quadrature over the element by using an a-priori error estimator similar to [33]. The number of quadrature nodes is determined by the smallest  $m$  for which all of the 3 a-priori error estimates

$$\begin{aligned}\varepsilon_G &:= 32 \left( \frac{1}{2\tilde{r}} \right)^{2m+1}, \\ \varepsilon_H &:= 64(2m+1) \left( \frac{1}{2\tilde{r}} \right)^{2m+2}, \\ \varepsilon_E &:= 128(m+1)(2m+1) \left( \frac{1}{2\tilde{r}} \right)^{2m+3}\end{aligned}$$

are smaller than the default tolerance of  $10^{-3}$ . If  $m$  becomes larger than 6,  $m$  is set to 6, which provides a compromise between accuracy and computational effort. Because of the splitting of elements into subelements done in the quasi-singular case,  $m = 6$  is a feasible upper limit even in the regular quadrature.

For quadrilateral elements, the quadrature nodes are given by the cross product of  $m \times m$  Gauss nodes on the interval  $[-1, 1]$ , [34]. For triangular elements, Gauss quadrature formulas for triangles based on  $m$  are used [35, 36].

### 3.2. Linear System of Equations Solvers

NumCalc offers to choose between a direct solver (either from LAPACK [29], if NumCalc is compiled with LAPACK-support, or a slower direct LU-decomposition) or an iterative conjugate gradient squared (CGS) solver [30]. The iterative solver is preferred, because, the number of elements  $N$  is generally large for a feasible computation with a direct solver. When using the iterative solver, NumCalc offers to precondition the system matrix by applying either row-scaling or an incomplete LU-decomposition [37, Chapter 5]. However, even with preconditioning, if the elements or the geometry of the scatterer are irregular, the CGS solver may have robustness problems, yielding in convergence issues. Thus, when using the iterative solver,

*“Hint 5: Check if the iterative solver has converged.”*

### 3.3. The Fast Multipole Method

One drawback of the BEM is that the system matrix is densely populated, which makes numerical computations with even moderately sized meshes prohibitively expensive in terms of memory consumption and computation time. This dense structure is caused by the Green’s function  $\frac{e^{ik||\mathbf{x}-\mathbf{y}||}}{4\pi||\mathbf{x}-\mathbf{y}||}$ , because the norm  $||\mathbf{x}-\mathbf{y}||$  introduces a nonlinear coupling between every element  $\Gamma_j$  and every collocation node  $\mathbf{x}_i$ .

The FMM is based on a man-in-the-middle principle where the Green’s function  $G(\mathbf{x}, \mathbf{y})$  is approximated by a product of three functions

$$G(\mathbf{x}, \mathbf{y}) \approx G_1(\mathbf{x} - \mathbf{z}_1)G_2(\mathbf{z}_1 - \mathbf{z}_2)G_3(\mathbf{z}_2 - \mathbf{y}). \quad (13)$$

This splitting has the advantage, that the integral over the BEM elements  $\Gamma_j$  can be calculated independently of the collocation node  $\mathbf{x}_i$ , and thus can be reused multiple times. On the downside, this splitting is only numerically stable if  $\mathbf{x}$  and  $\mathbf{y}$  are sufficiently apart from each other (for more details we refer to Sec. 3.3.1).

To derive this splitting, the elements of the mesh are grouped into different clusters  $\mathcal{C}_i$ . A cluster is a collection of elements that are within a certain distance of each other and for each cluster  $\mathcal{C}_i$  its midpoint  $\mathbf{z}_i$  is defined as the average over the coordinates of all vertices of the elements in the cluster. For two clusters  $\mathcal{C}_i$  and  $\mathcal{C}_j$  with  $\mathbf{z}_i$  and  $\mathbf{z}_j$  that are sufficiently “far” apart, the element-to-element interactions of all the elements between both clusters are reduced to the local interactions between each elements of a cluster with its midpoint (functions  $G_1$  and  $G_3$ ), and the interactions between the two clusters (function  $G_2$ ), respectively (cf. Fig. 3). Note that local-to-cluster and the cluster-to-cluster expansions can be calculated independently from each other.

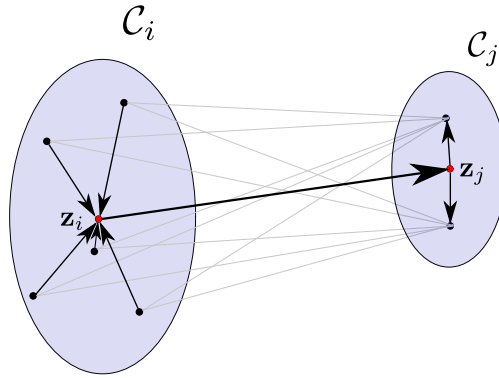


Figure 3: Scheme of a FMM interaction between two clusters. The interactions (gray lines) between elements (black dots) located in two distant clusters (shaded areas) are reduced to fewer within and between cluster interactions (black lines).

### 3.3.1. The expansion of the Green’s function

The expansion of the Green’s function is based on its representation as a series [38]:

$$\begin{aligned}
 G(\mathbf{x}, \mathbf{y}) &= \frac{e^{ik\|\mathbf{x}-\mathbf{y}\|}}{4\pi\|\mathbf{x}-\mathbf{y}\|} = \\
 &= \frac{ik}{4\pi} \int_{\mathbb{S}^2} e^{ik(\mathbf{x}-\mathbf{z}_1+\mathbf{z}_2-\mathbf{y})\cdot\mathbf{s}} \sum_{n=0}^{\infty} i^n (2n+1) h_n(k\|\mathbf{z}_1-\mathbf{z}_2\|) P_n \left( k \frac{(\mathbf{z}_1-\mathbf{z}_2)\cdot\mathbf{s}}{\|\mathbf{z}_1-\mathbf{z}_2\|} \right) d\mathbf{s} \\
 &\approx \frac{ik}{4\pi} \int_{\mathbb{S}^2} \mathcal{S}(\mathbf{x}, \mathbf{z}_1, \mathbf{s}) \mathcal{D}_L(\mathbf{z}_1-\mathbf{z}_2, \mathbf{s}) \mathcal{T}(\mathbf{y}, \mathbf{z}_2, \mathbf{s}) d\mathbf{s},
 \end{aligned} \tag{14}$$

where

$$\begin{aligned}\mathcal{S}(\mathbf{x}, \mathbf{z}_1, \mathbf{s}) &= e^{ik(\mathbf{x}-\mathbf{z}_1)\cdot\mathbf{s}}, \quad \mathcal{T}(\mathbf{y}, \mathbf{z}_2, \mathbf{s}) = e^{ik(\mathbf{z}_2-\mathbf{y})\cdot\mathbf{s}}, \\ \mathcal{D}_L(\mathbf{z}_1, \mathbf{z}_2, \mathbf{s}) &= \sum_{n=0}^L i^n (2n+1) h_n(k\|\mathbf{z}_1-\mathbf{z}_2\|) P_n\left(k\frac{(\mathbf{z}_1-\mathbf{z}_2)\cdot\mathbf{s}}{\|\mathbf{z}_1-\mathbf{z}_2\|}\right),\end{aligned}$$

and  $h_n$  denotes the spherical Hankel function of order  $n$ ,  $P_n$  is given by the Legendre polynomial of order  $n$ , and  $\mathbb{S}^2$  denotes the unit sphere in 3D.

The integral over  $\mathbb{S}^2$  needs to be calculated numerically. To this end, the unit sphere  $\mathbb{S}^2$  is discretized using  $2L^2$  quadrature nodes  $\mathbf{s}_j, j = 1, \dots, 2L^2$ , where  $L$  is the length of the multipole expansion in Eq. (14). The elevation angle  $\theta \in [0, \pi]$  is discretized using  $L$  Gaussian quadrature nodes, for the azimuth angle  $\phi \in [0, 2\pi]$ ,  $2L$  equidistant quadrature nodes are used [4].

It is not trivial to find an adequate truncation parameter  $L$  for the sum in Eq. (14) and a lot of approaches have been proposed [4, 39]. On the one hand,  $L$  needs to be high enough to let the sum in Eq. (14) converge. On the other hand, a large  $L$  implies Hankel functions with high order, which become numerically unstable for small arguments. Thus, the FMM is not recommended if two clusters are close to each other. In [4], a semi-heuristic formula for finding the optimal  $L$  is given by

$$L = kd_{max} + 5 \ln(kd_{max} + \pi)$$

for single precision and

$$L = kd_{max} + 10 \ln(kd_{max} + \pi)$$

for double precision, where  $d_{max}$  is maximum distance  $\|(\mathbf{z}_i - \mathbf{y}) + (\mathbf{x} - \mathbf{z}_j)\|$  over all clusters. As  $L$  depends also on the wave number  $k$ , the order of the FMM is also frequency dependent. NumCalc uses a similar bound:

$$L = \max(8, 2r_{max}k + 1.8 \log_{10}(2r_{max}k + \pi)), \quad (15)$$

where  $r_{max}$  is the radius<sup>1</sup> of the largest cluster. Our numerical experiments have shown that a lower bound for  $L$  can enhance the stability and accuracy (especially at lower frequencies) and that a factor of 1.8 is a good compromise between stability, accuracy, and efficiency. In Sec. 5 we present an example where a bigger factor was used to increase the accuracy of the BEM solution in a special case.

In Eq. (14), the functions  $\mathcal{S}$  and  $\mathcal{T}$  represent the local element-to-cluster expansion inside each cluster, whereas the function  $\mathcal{D}_L$  represents the cluster-to-cluster interaction. One key element in  $\mathcal{D}_L$  are the spherical Hankel functions  $h_n$  of order  $n = 0, \dots, L$ , that become singular at 0,  $\lim_{x \rightarrow 0} h_n(x) = O\left(\frac{1}{x^{n+1}}\right)$  [34]. Thus, the FMM expansion is only stable for relatively large arguments  $k\|\mathbf{z}_1 - \mathbf{z}_2\|$ , which implies that the FMM

---

<sup>1</sup>The radius of a cluster is the biggest distance between the vertices in the cluster and the cluster midpoint.

can only be applied for cluster-pairs that are sufficiently apart from each other. To this end, following [39], NumCalc analyzes the relation between the distance  $\|\mathbf{z}_i - \mathbf{z}_j\|$  of the cluster midpoints to their radii  $r_i$  and  $r_j$ , which are given by the maximum distance between the cluster midpoint and the vertices of the cluster elements. If

$$\|\mathbf{z}_i - \mathbf{z}_j\| > \frac{2}{\sqrt{3}}\|r_i + r_j\|, \quad (16)$$

the two clusters are defined to be in each others farfield and the FMM expansion is applied.

If two clusters do not fulfil Eq. (16), the clusters and their elements are defined to be in each others nearfield. The interaction between such cluster pairs will be calculated using the conventional BEM approach with the non-separable  $G(\mathbf{x}, \mathbf{y})$  leading to the sparse nearfield matrix  $\mathbf{N}$ . If two clusters are found to be in each others farfield, the Green's function  $G(\mathbf{x}, \mathbf{y})$  will be approximated by Eq. (14).

Note, that based on Eq. (14), the expansions for the derivatives of  $G$  are easy, because  $\mathbf{x}$  and  $\mathbf{y}$  only occur as arguments of exponential functions, for which the calculation of the derivative is trivial.

### 3.3.2. Cluster generation

To actually generate the clusters in NumCalc, a bounding box is put around the mesh. This box is then subdivided into (approximately) equally sized sub-boxes for which the average edge length can be provided by the user. Note, that the sub-boxes have the same edge length in all three dimension, thus, the number of sub-boxes may vary along the different coordinate axes.

If the edge length is not specified, the default edge length will be  $|e_b| = (\sqrt{N}A_0)^{1/2}$ , where  $N$  is the number of elements and  $A_0$  is the average area of all elements. The number of subdivisions is estimated by rounding the quotient of the edge length of the original box and the target edge length. Thus, the actual edge lengths of the sub-boxes can slightly deviate from the target length  $|e_b|$ . If the midpoint of an element is within a sub-box, the element is assigned to the box, and all elements inside the  $i$ -th sub-box form the cluster element  $\mathcal{C}_i$ . The choice of initial edge length can be motivated by the following idea: First, it is assumed that all elements have roughly the same size. Secondly, the assumption of having about  $n_0 = \sqrt{N}$  clusters with about  $N_0 = \sqrt{N}$  elements in each cluster provides a nice balance between the number of the clusters and the number of elements in each cluster. If we assume that the surface of the scatterer is locally smooth, the elements in each cluster cover approximately a surface area of  $A_C = N_0A_0$ . As each cluster is fully contained in one bounding box, a good estimate for the edge length of such a box is  $\sqrt{A_C} = \sqrt{N_0A_0} = \sqrt[4]{N}\sqrt{A_0}$ . Note, that the assumption of having elements of roughly the same size, has an impact on the efficiency of the method, but also influences the stability of the FMM expansion. If the size of the elements inside a cluster varies to much, the local element-to-cluster expansions may run into numerical troubles, thus:

*“Hint 6: The elements should have approximately the same size, at least locally.”*

Sub-boxes that contain no elements are discarded. Clusters with a small radius (in comparison with the average cluster radius) are merged with the nearest cluster with large size.

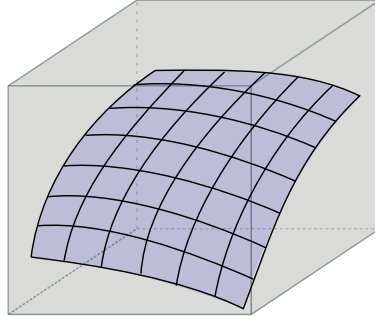


Figure 4: Example of a cluster (blue) and the bounding (sub)box (grey) around it.

Note, that there is a logical difference between the sub-box and the cluster. A cluster is just a collection of elements, which form a 2D manifold, whereas the bounding box is a full 3D object (see also Fig. 4). As a consequence, the radius of the cluster is usually *not* the same as half the edge length of the sub-box. Also, the cluster midpoint is usually different from the midpoint of the sub-box.

### 3.3.3. FMM System of Equations

Combining the FMM expansion Eq. (14) with the discretized BIE Eq. (10), the system of equations for the FMM has the form

$$\mathbf{N} + \mathbf{SDT}, \quad (17)$$

in which  $\mathbf{N}$  contains the contributions for cluster-pairs in the near-field where the FMM cannot be applied, and  $\mathbf{S}$ ,  $\mathbf{D}$  and  $\mathbf{T}$  contain the contributions of far-field cluster pairs, where the FMM expansion will be applied. Because of the clustering, the matrices  $\mathbf{S}$ ,  $\mathbf{D}$  and  $\mathbf{T}$  have a block-structure, see Fig. 5 for a schematic representation of block structure of  $\mathbf{SDT}$ .

To better illustrate the sparse structure of these matrices, we look at the entries of the different matrices with respect to the integral parts involving the Green's function  $G(\mathbf{x}, \mathbf{y})$ , the matrix parts for the integrals with respect to  $H$ ,  $H'$ , and  $E$  can be derived in a similar way.

The entries of the near-field matrix  $\mathbf{N}$  are calculated for each collocation node  $\mathbf{x}_i$  using the quadrature techniques for standard BEM (see Sec. 3.1), resulting in

$$\mathbf{N}_{ij} = \begin{cases} \int_{\Gamma_j} G(\mathbf{x}_i, \mathbf{y}) d\mathbf{y} & \Gamma_j \in \mathcal{N}_i, \\ 0 & \text{otherwise,} \end{cases}$$

where  $\Gamma_j$  is in the nearfield  $\mathcal{N}_i$  of the cluster containing the collocation node, and  $i, j = 1, \dots, N$ .

$$\left( \begin{array}{c} \boxed{\mathbf{S}_1} \\ \vdots \\ \boxed{\mathbf{S}_{2L^2}} \end{array} \right) \left( \begin{array}{ccc} \boxed{\mathbf{D}_1} & 0 & 0 \\ 0 & \ddots & 0 \\ 0 & 0 & \boxed{\mathbf{D}_{2L^2}} \end{array} \right) \left( \begin{array}{c} \boxed{\mathbf{T}_1} \\ \vdots \\ \boxed{\mathbf{T}_{2L^2}} \end{array} \right)$$

Figure 5: Block structure of the FMM matrices in the SLFMM. Each matrix block  $\mathbf{S}_i$  has size  $N \times N_C$ , where  $N$  is the number of elements and  $N_C$  is the number of clusters. Each block  $\mathbf{D}_i$  has size  $N_C \times N_C$  and each block  $\mathbf{T}_i$  has size  $N_C \times N$ .

The matrix  $\mathbf{D}$  represents the cluster-to-cluster interaction between Clusters  $\mathcal{C}_m$  and  $\mathcal{C}_n$ . It contains  $2L^2$  blocks of size  $N_C \times N_C$  defined by

$$(\mathbf{D}_\nu)_{mn} := \begin{cases} \mathcal{D}_L(\mathbf{z}_m, \mathbf{z}_n, \mathbf{s}_\nu) & \text{if } (\mathcal{C}_m, \mathcal{C}_n) \text{ is a far-field cluster pair,} \\ 0 & \text{otherwise,} \end{cases}$$

where  $N_C$  is the number of clusters,  $m, n = 1, \dots, N_C$ , and  $\nu = 1, \dots, 2L^2$ , with  $2L^2$  being the number of quadrature nodes on the unit sphere. Thus, the total size of  $\mathbf{D}$  is  $2N_C L^2 \times 2N_C L^2$ .

The matrix  $\mathbf{T}$  describes the local element-to-cluster expansion from each element to cluster's midpoint and is represented as a  $2L^2 \times 1$  dimensional block matrix

$$\mathbf{T} = (\mathbf{T}_1, \dots, \mathbf{T}_{2L^2})^\top,$$

where each single block has size  $N_C \times N$  and is defined by

$$(\mathbf{T}_\nu)_{mj} = \begin{cases} \int_{\Gamma_j} e^{i(\mathbf{z}_m - \mathbf{y}) \cdot \mathbf{s}_\nu} d\mathbf{y} & \Gamma_j \in \mathcal{C}_m, \\ 0 & \text{otherwise.} \end{cases}$$

The local distribution matrix  $\mathbf{S}$  of size  $1 \times 2L^2$  is defined by

$$\mathbf{S} = (\mathbf{S}_1, \dots, \mathbf{S}_{2L^2}),$$

where each  $N \times N_C$  block has the form

$$(\mathbf{S}_\nu)_{in} = \begin{cases} w_\nu e^{i(\mathbf{x}_i - \mathbf{z}_n) \cdot \mathbf{s}_\nu} & \mathbf{x}_i \in \mathcal{C}_n, \\ 0 & \text{otherwise,} \end{cases}$$

where  $w_\nu$  is the  $\nu$ -th weight used by the quadrature method for the integral over the unit sphere.

### 3.3.4. Multi level FMM (MLFMM)

For higher efficiency, the FMM also can be used in a multilevel form, in which a cluster tree is generated, i.e., the mesh is subdivided not only once into clusters in the first level (root level), but clusters are iteratively

subdivided in the next level, until the clusters at the finest level (leaf level) have about 25 elements. As the FMM is based on multiple levels, we speak of the multilevel fast multipole method (MLFMM) compared to the single level fast multipole method (SLFMM) described in Sec. 3.3.2.

In contrast to other implementations of the MLFMM where the cluster on the root level contains all elements of the mesh, in NumCalc, the root of the cluster tree is based on a clustering similar to that done in the SLFMM (see Sec. 3.3.2). In NumCalc, users can either define an initial bounding box edge length  $|e_r|$  or use the default target edge length chosen such that each cluster contains approximately  $N_0 = 0.9\sqrt{N}$  elements. As in the SLFMM, it is assumed that the elements have similar sizes with an area of  $A_0$  and an average edge length of  $|e_0|$ .

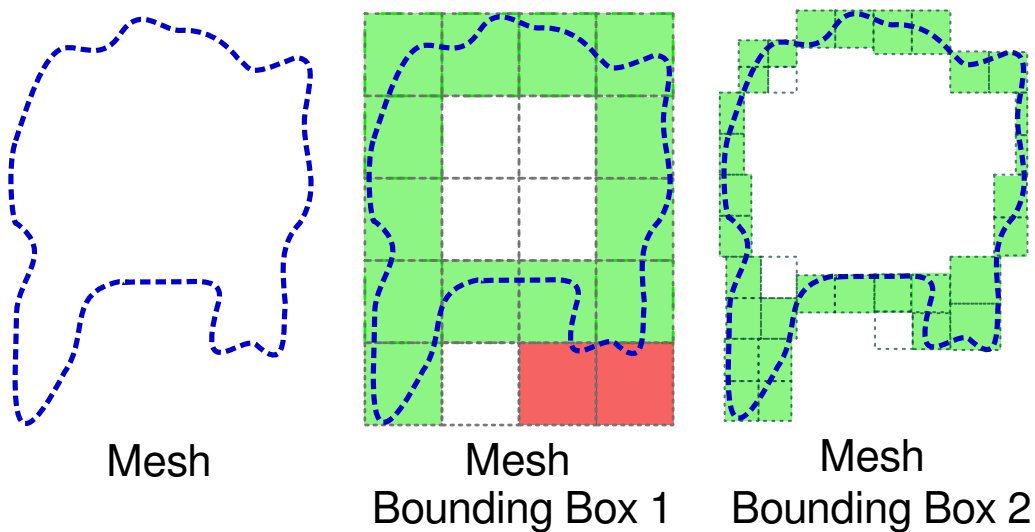


Figure 6: Example of the MLFMM clustering: Mesh (dark/blue line) and the bounding boxes for the first two levels. At each level, empty (white) boxes are discarded, small (dark grey/red) boxes are merged into the neighbouring large (light grey/green) boxes, which are used for the clustering.

The clusters at higher levels are constructed in two steps: First, new bounding boxes are created for each cluster based on the coordinates of element vertices in the respective cluster. Then, sub-boxes with target edge length  $\frac{|e_r|}{2^\ell}$  are created similar to the root level, where  $\ell$  is the number of the level. The elements within these sub-boxes then form the clusters in the new level of the MLFMM. The clusters contained in the sub-boxes in the new level are called children, the original cluster element is called parent cluster. Fig. 6 shows an example of creating the bounding boxes and clusters for the root and next level.

Currently, NumCalc does *not* build the cluster tree adaptively, but the number of levels

$$\ell_{\max} = \max \left( 1, \text{round} \left[ \log_2 \left( \frac{|e_r|}{|e_1|} \right) \right] \right) = \max \left( \text{round} \left[ \frac{1}{2} \log_2 \left( \frac{\sqrt{N}}{22.5} \right) \right] \right),$$

is determined beforehand, where  $|e_r|$  and  $|e_1|$  are the target bounding box lengths on the root and leaf level,

respectively. Because in the default setting, each cluster on the root level contains  $N_0 = 0.9\sqrt{N}$  elements, the edge length of each bounding box can be estimated by  $|e_r| = \sqrt{\frac{N}{N_0}}\sqrt{A}$ . On the leaf level, each bounding box contains about 25 elements, thus it has an edge length of  $|e_1| = 5\sqrt{A}$ . In that setting,  $\ell_{\max}$  defines how often  $|e_r|$  needs to be split to obtain  $|e_1|$ . NumCalc produces cluster trees which are well-balanced and where all leaf clusters are on the same level. Note, however, that the bounding boxes are constructed to have about the same edge length in all directions, thus, if the mesh has large aspect ratios, the number of clusters in the respective dimension will differ.

In practice, elements are rarely distributed regularly inside the bounding boxes. Thus our clustering approach may lead to leaf clusters with very few elements on the one hand and clusters with more than 25 elements on the other hand. Our numerical experiments have shown that having already about  $\sqrt{N}$  clusters in the root level improves the stability and efficiency of the FMM, because, for example, the expansion length used by the FMM (see Sec. 3.3.1) is kept relatively low.

In order to solve the MLFMM case, nearfield and farfield cluster-pairs are defined on each level using the same rule as for the SLFMM. However, in contrast to the SLFMM, the FMM is *not* applied for all far-field cluster pairs on each level, but only to a specific sub-set, the so called interaction list. For each cluster  $\mathcal{C}_j$ , the interaction list  $I(\mathcal{C}_j)$  is defined as the elements in the child clusters of the near field clusters of the parent of  $\mathcal{C}_j$ .

Calculations for the MLFMM start at the leaf level  $\ell_{\max}$ . For each cluster  $\mathcal{C}_i^{\ell_{\max}}$  on this level, the near field matrix  $\mathbf{N}$  is calculated for all near field cluster pairs as in the SLFMM case (for example the blue box and the two red boxes in Fig. 7). The fast multipole expansion, however, is only applied between each cluster  $\mathcal{C}_i^{\ell_{\max}}$  and the clusters in the respective interaction list  $I(\mathcal{C}_i^{\ell_{\max}})$  (green boxes in Fig. 7 for the selected blue cluster box). All other cluster-pairings (white boxes) on this level are neglected.

For those pairs, the local element-to-cluster expansions at level  $\ell_{\max}$  are transformed into local element-to-cluster expansions with respect to the parent cluster in level  $\ell_{\max}-1$  (upward pass, blue box to parent blue box in Fig. 7). This transformation is necessary because the parent cluster has a different cluster midpoint and maybe a different multipole expansion length as the child. At this level no near-field components need to be calculated, because these have already been “covered” by the calculations at the level of the children. For each pairing of cluster  $\mathcal{C}_i^{\ell_{\max}-1}$  and clusters in its interaction list, the FMM is performed. For all other cluster pairs the local expansions are again passed on to the parent, and the procedure is repeated at the level above.

In summary, at each level  $\ell$ , the local element-to-cluster matrices  $\mathbf{T}(\ell)$ , the local cluster-to-element matrices  $\mathbf{S}(\ell)$ , and the cluster-to-cluster interaction matrices  $\mathbf{D}(\ell)$  will be calculated, and the final system for the MLFMM is given by

$$N(\ell_{\max}) + \sum_{\ell=1}^{\ell_{\max}} \mathbf{S}(\ell)\mathbf{D}(\ell)\mathbf{T}(\ell).$$

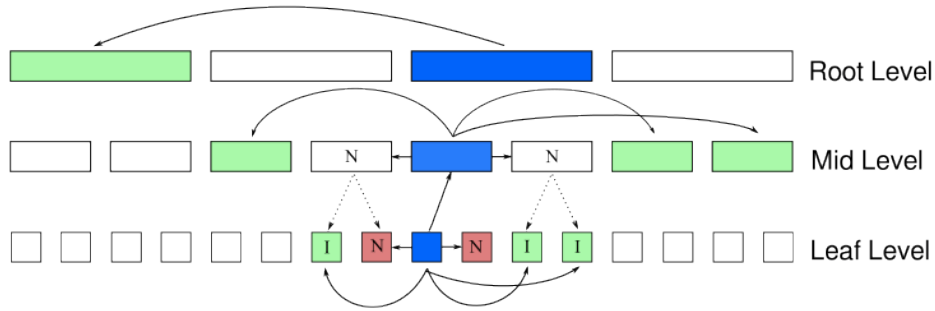


Figure 7: Scheme of the MLFMM. For a single cluster on the highest level  $\ell_{\max}$  (= leaf level, shown in the bottom row by the dark blue box), the red boxes denote its nearfield clusters and the light green boxes denote the clusters stored in the interaction list, for which the FMM is applied. The interaction with the other clusters within this level (denoted by the white boxes) are considered in the parent level  $\ell_{\max} - 1$ . This procedure is repeated for all levels of the MLFMM. Arrows depict interactions between clusters and messages passing to the parent, dotted arrows depict a parent-child relation.

While the MLFMM is recommended for most of the problems, NumCalc implements a few “safeguards” focused on an efficient calculation and stable results:

- If the user selects the conventional BEM (i.e., no FMM) but the number of elements  $N$  is larger than 20000, then NumCalc will still use the FMM, namely, the SLFMM.
- If the user selects the conventional BEM or the SLFMM, and the number of elements  $N$  is larger than 50000, then NumCalc will automatically switch to the MLFMM.
- If the user selects the FMM, but the wavelength  $\lambda$  is 80 times larger (or more) than the maximum distance  $r_{\max}$  between two nodes of the mesh, then NumCalc will still use the conventional BEM (i.e., *without* the FMM). This may especially be the case at low frequencies and prevents the too small truncation of the multipole method (see Section 3.3.1).
- If the user selects the MLFMM, but  $\lambda$  is larger than  $r_{\max}$  then NumCalc automatically switches back to the SLFMM.

One specific detail in NumCalc is the fact, that NumCalc determines the matrices  $\mathbf{T}(\ell)$ ,  $\mathbf{D}(\ell)$  and  $\mathbf{S}(\ell)$  beforehand for *all* levels and explicitly keeps those sparse matrices in memory. This is in contrast to many other implementations of the FMM, that only calculate the expansions on the leaf level, and then pass the information between levels by interpolation and filtering algorithms (cf. [40]). The approach in NumCalc has the advantage of a faster calculation because no interpolation and filtering routines are necessary for a slightly higher memory consumption at least for mid-size problems.

Nevertheless, one drawback of storing  $\mathbf{T}(\ell)$  and  $\mathbf{S}(\ell)$  on each level  $\ell \leq \ell_{\max}$  is that these matrices may become large close to the root level, which can cause problems with memory consumption. The radii of the clusters are larger at smaller levels (close to the root of the cluster tree), and thus the truncation parameter  $L$  in the multipole expansion (see Eq. (15)) and, in turn, the number of necessary quadrature nodes for the integral over the unit sphere increases when getting closer to the root. This implies that the number of blocks in  $\mathbf{T}(\ell)$  and  $\mathbf{S}(\ell)$  also increases towards the root, which means higher memory consumption. However, with the default of about  $\sqrt{N}$  clusters at root level, large clusters can be usually avoided and the memory consumption can be kept at a feasible level.

### 3.3.5. Memory estimation SLFMM

The number of non-zero entries of the nearfield matrix  $\mathbf{N}$  in Eq. (17) is given by the product of the number of interactions between the elements of two clusters, the number of possible nearfield clusters for a cluster, and the number of all possible clusters. As every cluster has about  $\sqrt{N}$  elements, a single nearfield cluster-to-cluster interaction adds  $N$  non-zero entries to the nearfield matrix. In the SLFMM the number of clusters is about  $\sqrt{N}$ , in the worst case, each cluster has 27 clusters in its nearfield, because a bounding box shares at least a face, an edge, or a vertex with 27 boxes (including itself). Therefore, in the worst case, the nearfield matrix  $\mathbf{N}$  has  $27N^{3/2}$  non-zero entries. However, one has to distinguish between the 3D bounding box and the cluster itself (see also Fig. 4). In practice, one can assume that each cluster has on average about 9 to 10 nearfield clusters. For most calculations, it is fair to assume that the matrix has about  $9N^{3/2}$  to  $10N^{3/2}$  non-zero entries. This assumption works well for small clusters where the surface of the scatterer inside the cluster has only little curvature. For more complex geometries and larger clusters, more non-zero entries are necessary.

The cluster in Fig. 4, for example, would probably have 9 clusters in its nearfield, one for each edge and each vertex of the cluster patch plus the patch itself. However, especially at lower cluster levels with bigger cluster radii, the assumption of low curvature is not always correct. In this case, the number of nearfield cluster can become larger than 9 or 10.

The local element-to-cluster expansion matrices  $\mathbf{T}$  and  $\mathbf{S}$  both have exactly  $2L^2N$  non-zero entries, where  $2L^2$  is the number of quadrature points on the sphere that depends on the truncation parameter  $L$ . As each element lies in exactly one cluster, there is only one local interaction between element and cluster midpoint, thus there are  $N$  local element-to-cluster expansions. Therefore, the number of  $2L^2N$  non-zero entries.

For the cluster-to-cluster interactions (matrix entries of  $\mathbf{D}$ ), it is assumed that each cluster has about 9 clusters in the nearfield. The number of non-zero entries of the midpoint-to-midpoint matrix is a product of number of clusters, number of far-field clusters, and the number of quadrature nodes on the unit sphere. On average  $\sqrt{N}(\sqrt{N} - 9)2L^2$  non-zero entries can be expected in total. The accuracy of this estimation depends on the uniformness of the discretization and the smoothness of the scattering object.

### 3.3.6. Memory Estimation MLFMM

We assume that the scatterer has a regular geometry without many notches and crests, thus each cluster can be assumed to have about 9 to 10 nearfield clusters, and although a parent box can be divided into 8 child-boxes, the same 2D manifold argument as above is used in the estimation that each parent has about 4 to 5 children.

In contrast to the SLFMM, the non-zero entries of the nearfield matrix  $\mathbf{N}$  now depend on the number of clusters on the highest (leaf-)level and the (average) number of elements in the leaf clusters. The number of non-zero entries on the leaf level can be estimated by the product of the number of clusters at the leaf level, the number of element-to-element interactions between two clusters, and the number of nearfield clusters. Therefore, the nearfield matrix  $\mathbf{N}$  has about  $\frac{N}{25} \cdot 25^2 \cdot 9 = 225N$  entries.

The local element-to-cluster expansion matrices  $\mathbf{T}(\ell)$  and  $\mathbf{S}(\ell)$  depend on  $L_\ell$ , the number of terms used in the multipole expansion. On a given level,  $\mathbf{T}(\ell)$  and  $\mathbf{S}(\ell)$  have exactly  $2L_\ell^2 N$  non-zero entries each.

On the root level, the number of non-zero entries of the midpoint-to-midpoint interaction matrix can be derived similar to the SLFMM. For higher levels, the number non-zero entries of  $\mathbf{D}(\ell)$  is given by the product of the number of clusters at the level, the number of quadrature nodes on the sphere, and the number of clusters in the interaction list of each cluster. Under the assumption that each cluster has about 4 children and about 10 neighbouring clusters (without the cluster itself), the number of non-zero entries for  $\mathbf{D}(\ell) \approx 4^{\ell-1} 0.9\sqrt{N} \cdot 2L_\ell^2 \cdot 40, \ell > 1$ . In Section 5.1.3 we will compare these estimates with the actual number of non-zeroes in the different multipole matrices for a simple example, which will show, that the estimates can only be rough estimates, because the assumptions about the number of clusters on each level is rather vague.

## 4. Critical components of NumCalc and Their Effect

While users may not be necessarily interested in the details covered in Sections 2 and 3, they should be aware of some of the consequences of the assumptions used in these sections and the key components of the BEM and the FMM.

### 4.1. Singularity of the Green's function

The Green's function  $G(\mathbf{x}, \mathbf{y})$  and its derivatives  $H(\mathbf{x}, \mathbf{y}), H'(\mathbf{x}, \mathbf{y}),$  and  $E(\mathbf{x}, \mathbf{y})$  are essential parts of the BEM. These functions become singular whenever  $\mathbf{x} = \mathbf{y}$ , i.e., when we integrate over the element  $\Gamma_i$  that contains the collocation point  $\mathbf{x}_i$ . There are algorithms that can deal with these type of singular integrals (cf. [31, 32]), but the singularities also cause *numerical* problems for elements in the neighbourhood of  $\Gamma_i$ . In NumCalc, these almost-singular integrals are calculated by subdividing the element several times (see also Section 3.1), but these subdivisions slow down calculations. The (almost) singularity especially causes problems if

- an external sound source is close to the surface of the object,
- there are very thin structures in the geometry, thus, if front and backside of the object are close to each other,
- there are overlapping or twisted elements.

If NumCalc terminates with an error code message “number of subels. which are subdivided in a loop must <= 15” the reason is most likely the presence of irregular or overlapping elements, causing more than 15 subdivisions of an element. NumCalc also displays the element index for which the error occurred. There is a high chance, that there is some problem with the mesh or an external sound source close to this element. So:

*“Hint 7: If you get a subdivision loop error, check your mesh in the vicinity of the element for overlaps and irregularities, or if there is a external sound source close to that element, move the source0 further away from the mesh.”*

#### 4.2. FMM matrices

The expansion Eq. (14) of the Green’s function has several consequences especially in connection with finding the right truncation length, see Section 3.3.1. For small arguments, the spherical Hankel function  $h_n(x) = j_n(x) + iy_n(x)$  of order  $n$  behaves like [34]

$$\lim_{x \rightarrow 0} j_n(x) = \frac{1}{1 \cdot 3 \cdot 5 \cdots (2n + 1)} x^n, \quad \lim_{x \rightarrow 0} y_n(x) = -\frac{1 \cdot 3 \cdot 5 \cdots (2n - 1)}{x^{n+1}}.$$

Thus, numerical problems may arise for large expansion lengths and small arguments because the spherical Hankel function goes to infinity with  $O(\frac{1}{x^{n+1}})$ . This is a problem, when  $k||z_1 - z_2|| \ll 1$ , which can happen at low frequencies and clusters being close to each other. The number of quadrature nodes on the sphere is a function of the truncation parameter  $L$ , which in turn means that the memory required to store the local-to-cluster expansion matrices  $\mathbf{T}$  and  $\mathbf{S}$  (having  $2L^2N$  non-zero entries) depends on  $L$ . As  $L$  depends on the cluster radius (e.g., Eq. 3.3.1) choosing the size of the initial bounding box has a huge effect on the memory requirement. The spherical Hankel functions are implemented with a simple recursive procedure [41, Section 3.2.1] with the aim to find a balance between accuracy and computation time. However, for higher orders, the calculations become more involved, and, as the calculation is based on a recursive formula, errors from lower orders propagate and add up at higher orders.

Hence, the length of the FMM expansion has a crucial effect on the results of the FMM. Thus:

*“Hint 8: If you need an expansion order  $L$  beyond 30, check the convergence of the iterative solver and then your results for plausibility.”*

If the large expansion length  $L$  causes problems, one remedy is to adjust the length of the initial bounding box such that the radii of the clusters decrease.

## 5. Benchmarks

In order to raise awareness on the limitations of NumCalc in terms of accuracy and computer resources, in the following, we present results for three benchmark problems in acoustics. First, we analyze the scattering of a planewave on a sound-hard sphere. Second, we analyze the calculation of the sound pressure on a human head caused by point-sources placed around the head. Finally, we analyze the calculation of the sound field inside a duct.

### 5.1. Sound-Hard Sphere

We consider the acoustic scattering of a plane wave on a sound-hard sphere with radius  $r = 1$  m. For this example, an analytic solution based on spherical harmonics [42, Chapter 7] is available for comparison for both on the surface and on points outside the sphere. To investigate the effect of various discretization methods, the meshes were created using two methods. The first type of meshes (cube-based meshes) was created by discretizing the unit cube with triangles and by projecting the discretized cube onto the unit sphere. The second type of mesh (icosahedron-based meshes) was the often-used construction using an (subdivided) icosahedron that is projected onto the sphere. Both meshes were discretized using triangles, thus, each element had a unique normal vector.

In general, the icosahedron-based meshes had almost equilateral triangular elements of about the same size, but the number of elements were restricted to  $N_{\text{ico}} = 20 \cdot 4^n, n \in \mathbb{N}_0$ . The number of elements for the cube-based meshes were only restricted to  $N_{\text{cube}} = 6 \cdot (n + 1)^2, n \in \mathbb{N}_0$ , but the triangles were not as regular as in the icosahedron-based meshes, and the size of the triangles differed over the sphere, especially near the projected edges of the cube. An example for both meshes is depicted in Fig. 8 where the sphere on the left side is based on a projected cube and has 5292 elements, and the mesh on the right is based on an icosahedron and has 5120 elements. In Section 5.1.1, the acoustic field for both spheres was calculated and the effect of the different discretizations are discussed.

In NumCalc, the acoustic field on the surface is calculated on the *collocation* nodes, which, in this example, do not lie on the surface of the unit sphere. Thus, the errors depicted here also contain some error introduced by the geometry. For that reason, we also compared the numerical solutions to the analytical solution for a sphere with a radius adjusted to the minimal distance of the collocation nodes to the center of the sphere. This has an effect on the errors reported here, but this effect was tiny because of the accurate discretization of the sphere by the triangles.

To illustrate the combination of incoming and scattered acoustic field and investigate the errors in the acoustic field outside the sphere, 24874 evaluation points have been placed on a plane around the sphere. Figure 9 shows the logarithmic sound pressure level (SPL) in dB as an example of such acoustic field calculated for two frequencies. These evaluation points were also used to compute the errors between the

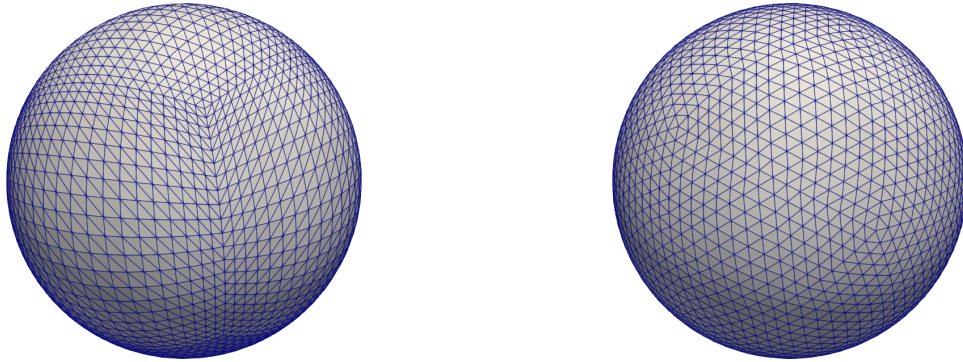


Figure 8: Discretizations of the unit sphere used in our benchmark. On the left side, the mesh was generated by discretizing a cube and projecting it onto a sphere. Note the smaller triangles close to the projected edges of the cube. On the right, the mesh is based on a subdivided and projected icosahedron.

BEM solution and the analytic solution outside the sphere. In the calculations, the MLFMM was used with the default settings.

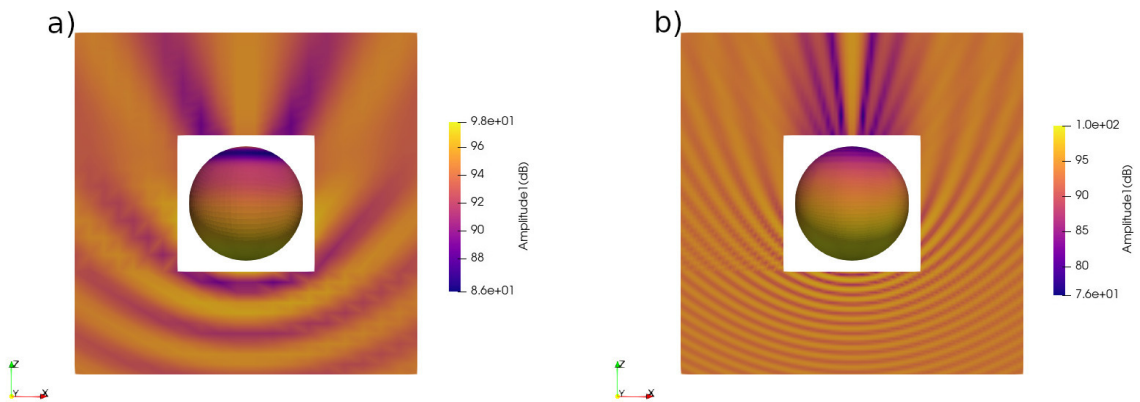


Figure 9: Example of the acoustic field calculated for 200 Hz (left panel) and 1000 Hz (right panel) caused by a plane wave in the  $z$ -direction.

### 5.1.1. Effect of element regularity

Fig. 10 shows the difference between the numerical and the analytical solutions, illustrating the effect of element regularity. The color represents the difference between the SPLs calculated at the midpoint of each element on the sphere. The effect is shown for the frequency of  $f = 800$  Hz and the two different types of

discretizations. Note that both meshes fulfil the 6-to-8-elements per wavelength rule for frequencies up to about 950 Hz.

Despite having a similar number of elements, the different regularity in the two meshes has a clear effect on the errors. For the very regular icosahedron-based triangularization, the errors between the calculated and the analytic SPLs were between  $\pm 0.34$  dB. For the cube-based triangularization, the errors were larger, i.e., between  $-0.7$  and  $0.9$  dB, being considerably larger at the triangles around the projected cube edges. In contrast to the icosahedron-based mesh, for the cube-based mesh, we observed a clearer distinction in the errors between the “sunny” and “shadow” side, i.e., the side oriented towards the plane wave and the side oriented away from the plane wave. For the icosahedron-based mesh, the error distribution was more smooth across the two sides.

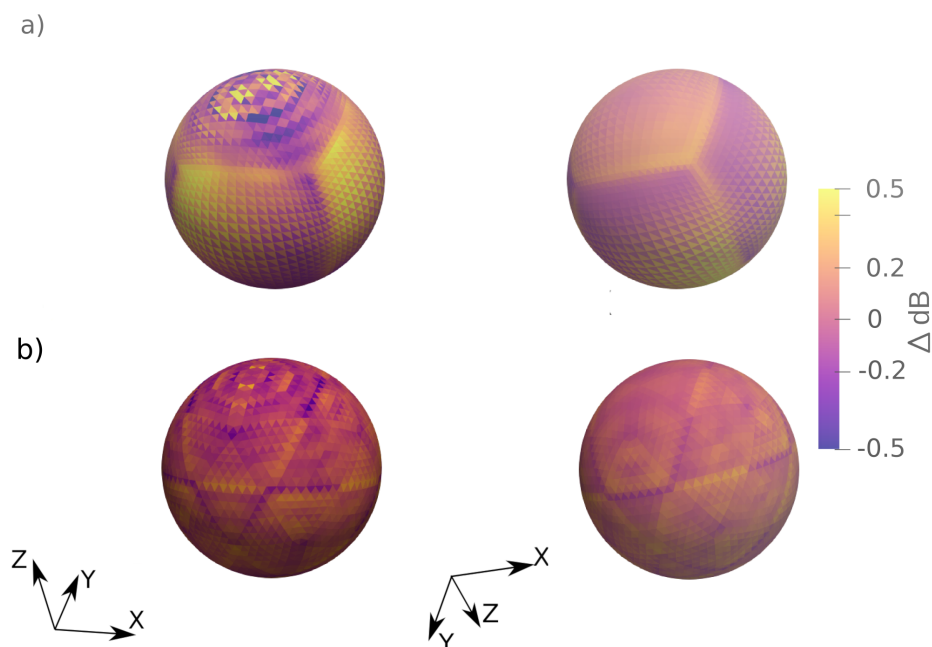


Figure 10: Sound pressure level differences (in dB) between the BEM calculation and the analytical solution at  $f = 800$  Hz. a) Cube-based mesh, b) Icosahedron-based mesh. As external source a plane wave in the negative  $z$  direction was used.

### 5.1.2. Error as function of the number of elements $N$

In this section, we analyzed the effect of the number of elements. To this end, we calculated the relative error

$$\varepsilon_r(\mathbf{x}) := \frac{|p(\mathbf{x}) - p_0(\mathbf{x})|}{|p_0(\mathbf{x})|}$$

between the calculated acoustic field  $p$  and the quasi-analytical solution  $p_0$  given in, e.g., [42, Chapter 7]. For the calculations, we considered the error on the surface as well as outside the sphere as a function of the

number of elements  $N$ . Further, we used the cube-based meshes only because the generation of the mesh based on the cube was more flexible in terms of available numbers of elements  $N$ .

Figs. 11 and 12 show the maximum, mean, and minimum of the relative errors calculated for the frequency of 200 and 1000 Hz, respectively. It is known, that the numerical error of the collocation method with constant elements is linearly proportional to the average edge length of the mesh. To illustrate this theoretical behaviour, the dotted line represents the functions  $\frac{1}{\sqrt{N}}$  which is roughly proportional to the average edge length of the elements. In principle, the errors are in the range of  $O(\frac{1}{\sqrt{N}})$ , however, for the lower frequency (Fig. 11), the errors increased with the number of elements. For NumCalc, it can be shown that this effect is caused by the following specific details of the implementation:

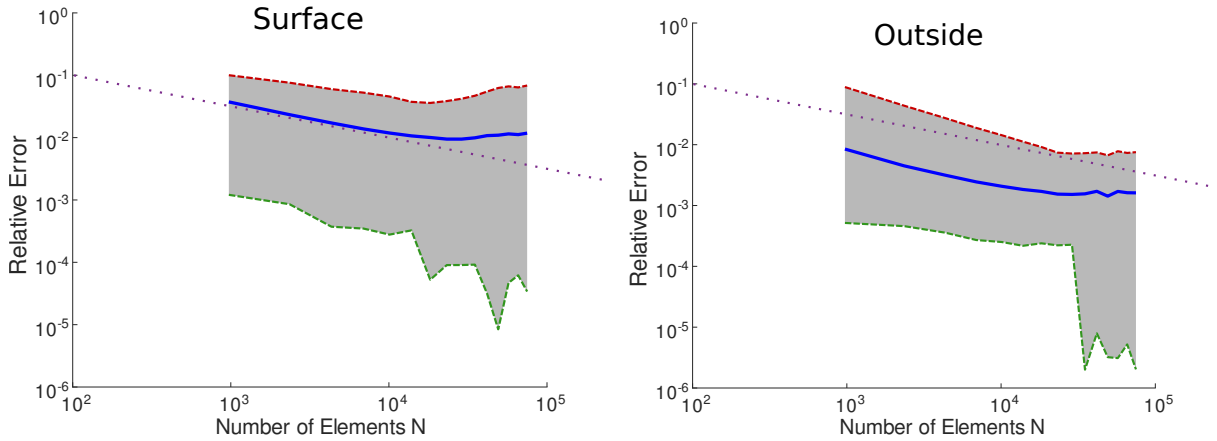


Figure 11: Relative errors as a function of the number of elements  $N$  for the sphere benchmark at  $f = 200$  Hz. Left side: Error on the surface of the sphere. Right side: Error around the sphere. The continuous (blue) line depicts the mean error over all nodes, the gray area depicts the area between the maximum and the minimum error (dashed lines). The dotted line depicts the function  $\frac{1}{\sqrt{N}}$ .

- For the integral over the boundary elements, the maximum order of the Gauss quadrature is six per default. For regular integrals, this is a good compromise between accuracy and efficiency. However, sometimes this maximum order can be too small for quasi-singular integrals, even after the subdivision procedure having applied (see Sec. 3.1).
- The factor determining the multipole expansion length is 1.8 per default (see Sec. 3.3.1). While, in the most cases, this default is sufficient for an accurate but fast calculation, for a better accuracy, it needs to be increased at for the price of a longer calculation.

In order to demonstrate the effect of the maximum order and the factor determining the multipole expansion length, we repeated the calculations, however, with two modifications of the parameters. First, the quasi-singular quadrature was modified such that each element was additionally subdivided, if the

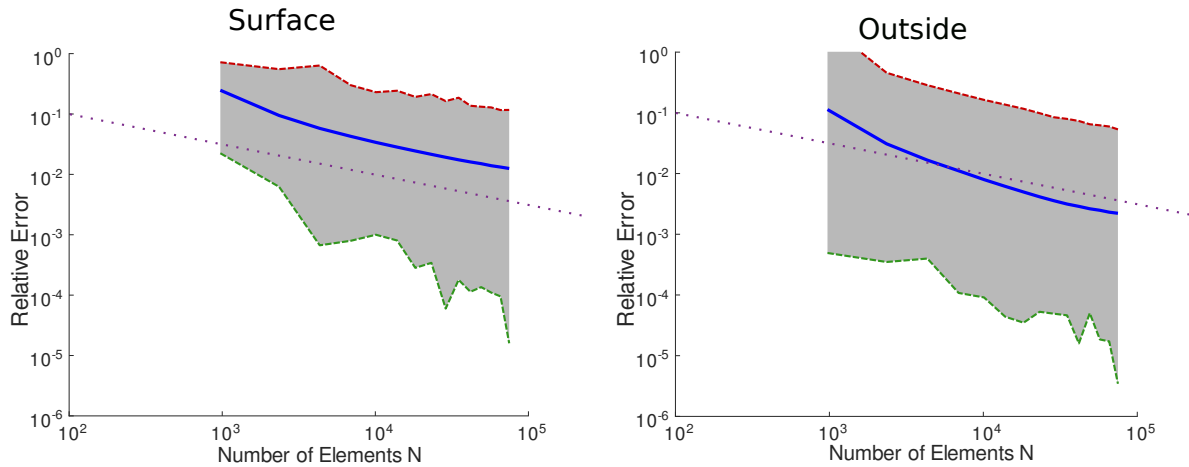


Figure 12: Relative errors as a function of the number of elements  $N$  for the sphere benchmark at  $f = 1000$  Hz. Left side: Error on the surface of the sphere. Right side: Error around the sphere. The continuous (blue) line depicts the mean error over all nodes, the gray area depicts the area between the maximum and the minimal error (dashed lines). The dotted line depicts the function  $\frac{1}{\sqrt{N}}$ .

estimated maximum order was larger than 6. Second, the factor determining the multipole expansion length was set to 15 (see Eq. (3.3.1)). This resulted in slightly higher multipole lengths  $L$ . For example, for a mesh with  $N = 74892$  elements, the truncation  $L$  calculated for the multipole levels of  $\ell = 1, 2$ , and 3 was  $L_{1,2,3} = 12, 10, 9$  (in opposite to  $L_{1,2,3} = 8, 8, 8$  obtained with the default setting), respectively. Fig. 13 shows the relative errors obtained with the modified parameter settings. As expected, the errors decreased showing a better accuracy of the calculations. Note that the additional accuracy was paid with the longer computation time. For example, for a mesh with  $N = 34992$  elements, the time to set up the linear system increased by factor *two to three* as compared to that obtained with default parameters.

This observation has several other implications. First, it is possible to achieve a higher accuracy in the calculations. This is however linked with the price of longer calculations, even though the calculation time might be still reasonable. In our example, the calculation time was still within 5 minutes even for the mesh with  $N = 74892$  elements. Further, users should ask themselves if the higher accuracy is actually required because the gain can be small (compare Fig. 13 vs Fig. 11). Finally, if optimizing for both speed and accuracy, a promising approach can be replacing the fine mesh with a coarser mesh at low frequencies.

### 5.1.3. Effect of the FMM

In this section, we analyzed the effect of FMM on the accuracy. To this end, we calculated the relative difference

$$\frac{|p_{\text{FMM}} - p_{\text{w/o FMM}}|}{|p_{\text{w/o FMM}}|}$$

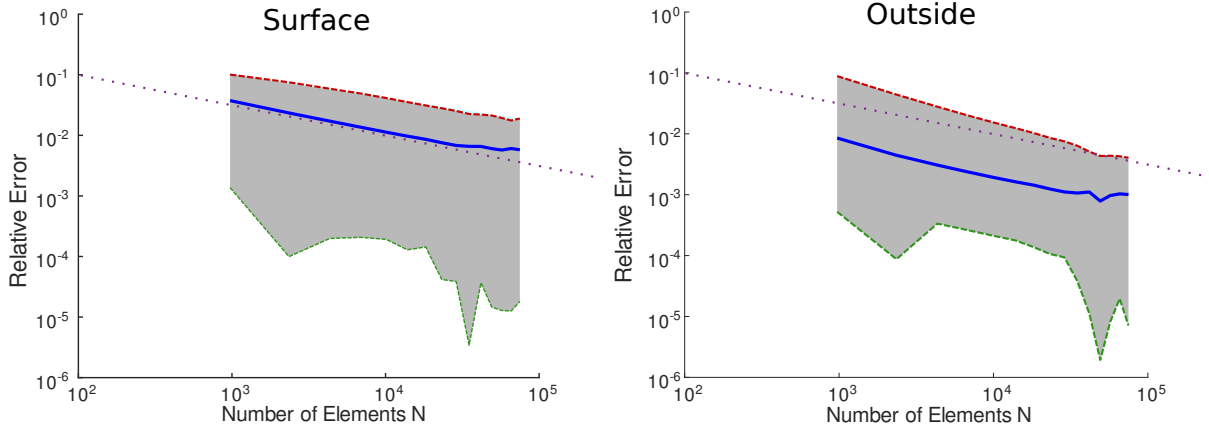


Figure 13: Relative errors with a higher accuracy setting as a function of the number of elements  $N$  for the sphere benchmark at  $f = 200$  Hz. Left side: Error on the surface of the sphere. Right side: Error around the sphere. The continuous (blue) line depicts the mean error over all nodes, the gray area depicts the area between the maximum and the minimal error (dashed lines). The dotted line depicts the function  $\frac{1}{\sqrt{N}}$ .

between the BEM calculations performed with and without the FMM. In the latter condition, we used a direct solver, i.e., `zgetrf` routine from LAPACK [29] and limited  $N$  to 8748 elements in order to keep the matrices at feasible sizes. The calculations were done for the frequencies 200 and 1000 Hz. Fig. 14 shows the

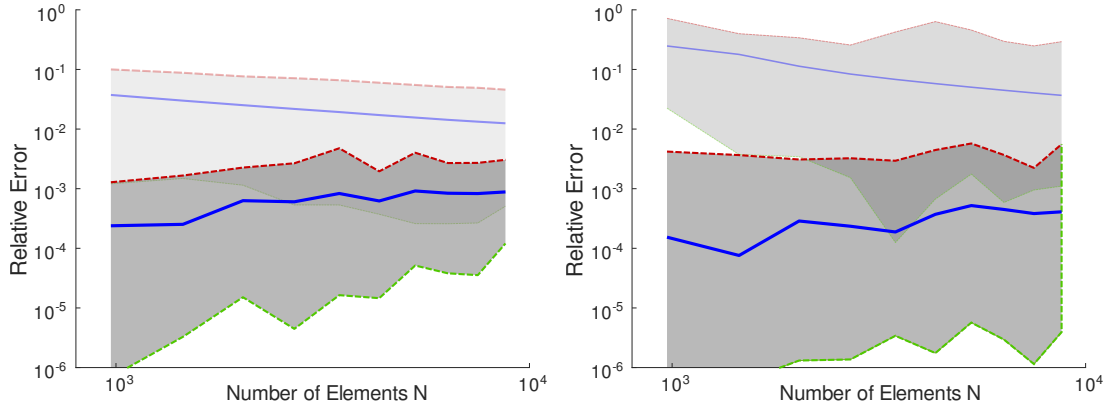


Figure 14: Relative error between BEM and analytic solution (lighter colors), and the relative distance of the BEM calculations with and without FMM at 200 Hz (a) and 1000 Hz (b) as function of the number of elements  $N$ . The dashed lines depicts the maximum and minimal relative distances between conventional BEM and FMM solution, the continuous (blue) lines the mean distance between both solutions.

relative errors obtained in the two conditions, calculated as a function of  $N$  for the two frequencies. This figure shows also the overall errors as compared to the analytic solution. The relative errors introduced by the FMM were in the range of  $10^{-3}$ , thus showing only a minor effect on the overall error. Note that at 1000 Hz (Fig. 14b), the wavelength is about 0.34 m, which means, that the 6-to-8 elements per wavelength

is only fulfilled for meshes with more than 6000 elements. This explains the large overall errors in Fig. 14b.

#### 5.1.4. Memory requirement: Moderate mesh size

In this section, we analyzed the memory requirements as an effect of the clustering. To this end, we compared the estimated and actual number of non-zero entries in the FMM matrices (see Sec. 4.2). We used the cube-based meshes and considered calculations for the frequency of 200 Hz for which we investigated the number of non-zero elements in the SLFMM and the MLFMM. We considered a unit sphere represented by a moderate size of  $N = 4332$  elements, for which the minimum, average, and maximum edge lengths was approximately 0.05 m, 0.09 m, and 0.15 m, respectively.

For the SLFMM, the clustering resulted in  $N_C = 90$  clusters, with the number of elements in a single cluster varying between 29 and 72 elements. Fig. 15 shows the mesh and visualizes the obtained clusters. The average number of elements per cluster was 48 elements, which is significantly different than the aimed estimation of  $\sqrt{N} \approx 65$ . This indicates that the actual clustering yields a different size even for a regular geometry such as the sphere. This difference has an impact on the estimation of the non-zero entries of the FMM matrices and thus the accuracy of the estimation for the memory requirement.

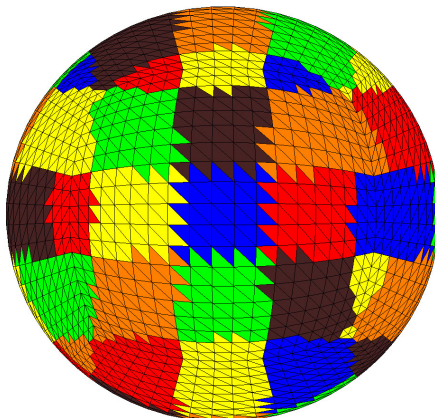


Figure 15: Example of default clustering for the unit sphere at 200Hz for a mesh with  $N = 4332$  elements. The different colors/gray scales depict different clusters.

For the SLFMM, Tab. 1 shows the information about the mesh and the clustering, as well the estimated and the actual numbers of non-zero entries of the FMM matrices. For the midpoint-to-midpoint matrix  $\mathbf{D}$ , two types of the estimations are shown: that based on the estimated number of clusters ( $\sqrt{N}$ ) and that based on the actual number of clusters ( $N_C$ ). It can be seen that the estimated non-zero entries of the midpoint-to-midpoint matrix  $\mathbf{D}$  are more accurate when using the actual number of clusters. Also the

estimate gets better, if on average 10 instead of 9 neighbouring clusters (including the cluster itself) are assumed, but this number depends on the individual mesh. Note that in these calculations, the truncation parameter of the SLFMM expansion length (see Eq. 15) was  $L = 8$ . While at a frequency of 200 Hz, Eq. (15) would result in  $L = 4$ ,  $L$  was increased to  $L = 8$  because numerical experience showed that  $L = 8$  is a good compromise between numerical effort, accuracy, and stability in the low frequency region.

Cluster Info		Matrix	Actual	Estimate
Nr. Boundary Elems	$N = 4332$	<b>N</b>	2 700 492	$10(\sqrt{N})^3 \approx 2\,851\,323$
Nr. Clusters	$N_C = 90$	<b>T, S</b>	554 496	$2L^2 N = 554\,496$
Truncation	$L = 8$	<b>D</b>	907 520	$2L^2\sqrt{N}(\sqrt{N} - 10) \approx 470\,249$ $2L^2 N_C(N_C - 10) = 921\,600$

Table 1: Basic information about the mesh and the clustering for the SLFMM example and the estimated and actual number of non-zero entries of the FMM matrices.

For the MLFMM, the clustering yielded  $\ell_{\max} = 2$  levels. At the root level, we obtained  $N_C^{[1]} = 56$  clusters, with the smallest, average, and maximum number of elements in an individual cluster being 30, 73, and 104 elements, respectively. The estimated number of clusters at the root level was  $N_{C,\text{est}}^{[1]} = 0.9\sqrt{N} \approx 59$ . At the leaf level, we obtained  $N_C^{[2]} = 252$  clusters, with the minimum, average, and maximum number of elements in a cluster being 2, 17, 30 elements, respectively. The low number of elements demonstrates the effect of subdividing all parents on each level. On both levels, the expansion length was  $L_1 = L_2 = 8$ . Tab. 2 shows the information about the clustering and the number of actual and estimated non-zero entries. For the estimation, it was assumed that each cluster has 10 clusters in its nearfield and that each parent has 4 children. For the cluster-to-cluster matrices **D**<sub>1</sub> and **D**<sub>2</sub>, estimations based on both the estimated number of clusters ( $\sqrt{N}$ ) and the actual number of clusters ( $N_C$ ) are shown. The results show that even the estimates based on the number of elements  $N$  are well approximating the actual number of non-zero elements.

Cluster Info		Matrix	Actual	Estimate
Nr. Boundary Elems	$N = 4332$	<b>N</b>	931 200	$10 \cdot 25^2 \cdot N/25 = 1\,083\,000$
Nr. Clusters	$N_C^{[1]} = 56$	<b>T<sub>ℓ</sub>, S<sub>ℓ</sub></b>	554 496	$2L^2 N = 554\,496$
	$N_C^{[2]} = 252$	<b>D</b> <sub>1</sub>	327 680	$2L^2 N_{C,\text{est}}^{[1]} (N_{C,\text{est}}^{[1]} - 10) \approx 370\,048$
Truncation	$L_1 = 8$			$2L^2 N_C^{[1]} (N_C^{[1]} - 10) = 329\,728$
	$L_2 = 8$	<b>D</b> <sub>2</sub>	1 193 984	$2L^2 \cdot N/25 \cdot 10 \cdot 4 \approx 887\,194$ $2L^2 \cdot N_C^{[2]} \cdot 10 \cdot 4 = 1\,290\,240$

Table 2: Basic information about the mesh and the clustering and estimated and actual number of non-zero entries of the MLFMM matrices.

### 5.1.5. Memory requirement: Large mesh size

In this section, we repeated the analysis, however, using a mesh with more elements, i.e., the sphere was represented by  $N = 8112$  elements. With such a discretization, the minimum, average, and maximum edge lengths of all boundary elements was about 0.06, 0.04, and 0.118 m, respectively.

For the SLFMM, Tab. 3 shows the clustering information and the estimations. The clustering resulted in  $N_C = 90$  clusters, with the number of elements in individual clusters ranging from 52 to 144 elements. Note that the estimation for the number of clusters  $N_C = \sqrt{N}$  is quite accurate. When compared to the previous mesh with only half of the elements, it might appear surprising that despite the higher number of elements, the number of clusters did not increase. Note, however, that for the SLFMM, the number of clusters is per default determined on  $\sqrt{N}$  bounding boxes, thus the difference in the number of clusters between the two sizes of the meshes is quite small. And one has to distinguish between the bounding box and the cluster inside this box. The estimation of the non-zero entries of  $\mathbf{N}$  was slightly smaller than the actual number. When assuming that the nearfield for each cluster contains on average 12 clusters (including itself), the estimation was more close to the actual number.

Cluster Info		Matrix	Actual	Estimate
Nr. Boundary Elems	$N = 8112$	$\mathbf{N}$	8 678 432	$10(\sqrt{N})^3 \approx 7\,306\,206$
Nr. Clusters	$N_C = 90$			$12(\sqrt{N})^3 \approx 8\,767\,447$
Truncation	$L = 8$	$\mathbf{T}, \mathbf{S}$	1 038 336	$2L^2N = 1\,038\,336$
		$\mathbf{D}$	911 616	$2L^2\sqrt{N}(\sqrt{N} - 10) \approx 923\,050$

Table 3: Basic information about the clustering and the comparison between estimated and actual number of non-zero entries of the SLFMM matrices.

For the MLFMM, Tab. 4 shows the clustering results and the estimations. At the root level, the clustering yielded  $\ell_{\max} = 2$  levels, with  $N_C^{[1]} = 90$  clusters, with the number of elements inside the individual clusters ranging from 52 to 144 elements and, on average, each cluster containing 90 elements. On the leaf level,  $N_C^{[2]} = 360$  clusters were created, with the number of elements in the individual clusters being between 4 and 54 elements and the average number of elements per cluster being 23 elements. At both levels, the expansion length of the MLFMM expansion was  $L_1 = L_2 = 8$ . The estimates for the nearfield matrix was slightly too small, but in overall, the estimates matched well the actual numbers, if the actual number of clusters was considered.

### 5.1.6. Memory requirement: Bounding box length

In this section, we investigated the effect of changing the initial length of the bounding box. To this end, the sphere was represented by  $N = 8112$  elements as in the previous example, but the the initial length

Cluster Info		Matrix	Actual	Estimate
Nr. Boundary Elems	$N = 8112$	$\mathbf{N}$	2 403 648	$10 \cdot 25^2 \cdot N/25 = 2\,028\,000$
Nr. Clusters	$N_C^{[1]} = 90$	$\mathbf{T}_\ell, \mathbf{S}_\ell$	1 038 336	$2L^2 N = 1\,038\,336$
	$N_C^{[2]} = 360$	$\mathbf{D}_1$	911 616	$2L^2 \cdot N_{C,\text{est}}^{[1]} (N_{C,\text{est}}^{[1]} - 10) \approx 736\,128$
Truncation	$L_1 = L_2 = 8$			$2L^2 \cdot N_C^{[1]} \cdot (N_C^{[1]} - 10) = 921\,600$
		$\mathbf{D}_2$	1 747 968	$2L^2 \cdot N/25 \cdot 10 \cdot 4 \approx 1\,661\,337$
				$2L^2 \cdot N_C^{[2]} \cdot 10 \cdot 4 = 1\,843\,200$

Table 4: Basic information about the clustering and the comparison between estimated and actual number of non-zero entries of the MLFMM matrices.

of the bounding box at the root level was set to 0.7m. For the estimation of the non-zero entries of the FMM matrices the actual number of clusters generated by NumCalc in the calculation were used.. The calculations were done with the SLFMM only, for the cube-based meshes and the frequency of 200 Hz.

Tab. 5 shows the clustering results and the estimations. The clustering generated  $\ell = 3$  cluster levels. The root level consisted of  $N_C^{[1]} = 26$  clusters, with 312 elements per cluster on average, ranging between 184 and 370 elements per cluster. On the second level,  $N_C^{[2]} = 144$  clusters were generated, with 56 elements per cluster on average, ranging between 28 and 77 elements per cluster. On the leaf level,  $N_C^{[3]} = 536$  clusters were generated, with 15 elements per cluster on average, ranging between 1 and 32 elements per cluster. On each level, the expansion length was  $L_1 = L_2 = L_3 = 8$ .

This example illustrates that setting the bounding box length for the root level affects the clustering to a large degree. It affected the number of levels, the number of elements per cluster, and the radii of each cluster. By adjusting the initial length of the bounding boxes at the root level, the radii of each cluster can be controlled, and thus the length of the multipole expansion. This helps in controlling the number of non-zero entries in the matrices  $\mathbf{T}_\ell$  and  $\mathbf{S}_\ell$  to some extent.

Cluster Info		Matrix	Actual	Estimate
Nr. Boundary Elems	$N = 8112$	$\mathbf{N}$	1 525 972	$(N/n_3)^2 \cdot 10 \cdot N_C^{[3]} \approx 1\,225\,411$
Nr. Clusters	$N_C^{[1]} = 26$	$\mathbf{T}_\ell, \mathbf{S}_\ell$	1 038 336	$2L^2 \cdot N = 1\,038\,336$
	$N_C^{[2]} = 144$	$\mathbf{D}_1$	58 624	$2L^2 \cdot N_C^{[1]} \cdot (N_C^{[1]} - 10) = 53\,248$
	$N_C^{[3]} = 537$	$\mathbf{D}_2$	641 024	$2L^2 \cdot N_C^{[2]} \cdot 4 \cdot 9 = 663\,552$
Truncation	$L_1 = L_2 = L_3 = 8$	$\mathbf{D}_3$	2 334 864	$2L^2 \cdot N_C^{[3]} \cdot 4 \cdot 9 = 2\,469\,888$

Table 5: Basic information about the clustering and the comparison between estimated and actual number of non-zero entries of the MLFMM matrices. The initial sub-box length was set to 0.7 m, additionally it was assumed that each for each cluster the nearfield consists of 9 clusters.

### 5.2. MLFMM: Head and Torso

This example was chosen to illustrate some of the restrictions on the current implementation of the FMM in NumCalc. In this example, we look at a model of head and torso of a human consisting of 174 298 triangular elements. This mesh is used to calculate the reflection of sound waves at the human head, torso, and especially at the pinna. A point source was placed near the entrance of the pinna. There is also a large difference in the size of the elements between torso (relatively coarse discretization) and the human pinnae, where the discretization needs to be fine in order to correctly approximate the geometry and the solution. In this case the minimum, average, and maximum edge length of all boundary elements were 0.7, 3.3, and 6.7 mm, respectively. The default clustering results in 3 levels with  $N_C^{[1]}, N_C^{[2]}, N_C^{[3]} = 422, 1558, 6378$  clusters per level, the expansion length on each level is given by  $L_1, L_2, L_3 = 31, 19,$  and 11, respectively.

For this example, the amount of memory additionally used for storing the matrices  $\mathbf{T}_\ell$  and  $\mathbf{S}_\ell$  on each level becomes very large. Although, in theory, the additional memory requirements are only  $O(N)$ , the length of the expansion and thus the factor  $2L_\ell^2$  becomes relatively large. For this example the memory needed by the FMM matrices alone is about 30.1 GByte. The non-zero entries of  $\mathbf{T}_\ell$  and  $\mathbf{S}_\ell$  ( $\ell = 1, 2$ ) on levels  $\ell = 1$  and  $\ell = 2$  are about 61% of all non-zero entries of the FMM matrices, see Tab. 6. The additional memory needed to explicitly store these matrices could be avoided, e.g. by filtering/interpolation algorithms for the FMM matrices. In this case, the gain in computing time by avoiding filtering/interpolation between levels does not outweigh the additional memory consumption. Of course, compared to the  $O(N^2)$  memory needs of 486 GByte for the traditional BEM, the FMM is still very effective.

Cluster Info		Matrix	Entries
Nr. Boundary Elems	$N = 170\,914$	$\mathbf{N}$	74 412 824
Nr. Clusters	$N_C^{[1]} = 403$	$\mathbf{T}_1 = \mathbf{S}_1$	335 000 756
	$N_C^{[2]} = 1512$	$\mathbf{T}_2 = \mathbf{S}_2$	125 843 156
	$N_C^{[3]} = 6226$	$\mathbf{T}_3 = \mathbf{S}_3$	42 180 116
Truncation	$L_1 = 37$	$\mathbf{D}_1$	333 601 540
	$L_2 = 20$	$\mathbf{D}_2$	36 733 916
	$L_3 = 16$	$\mathbf{D}_3$	51 291 416

Table 6: Basic information about the clustering and number of non-zero entries of the MLFMM matrices for the head-and-torso model.

### 5.3. Duct problem

This problem is one of the benchmarks described in [43]. It describes the problem of calculating the acoustic field inside a closed sound-hard duct of length  $L = 3.4$  m that has a quadratic cross section with

an edge length of  $w = 0.2$  m. At the closed side at  $x = 0$ , a velocity boundary condition with  $v = 1$  m/s is assumed, at the closed side at  $x = L$  an admittance boundary condition with  $Y = \frac{1}{\rho c}$  is assumed, where  $\rho = 1.3$  kg/m<sup>3</sup> and  $c = 340$  m/s are the density and the speed of sound in the medium, respectively. The quadratic cross section has the advantage that the geometry of the duct can be modelled accurately. A mesh for this problem including the positions of evaluation nodes inside the duct is partly depicted in Fig. 16a. The solution for these boundary conditions is given by a plane wave inside the duct traveling from one end to the other

$$p(x) = -\rho c e^{ikx}, \quad (18)$$

for the given speed of sound and the given density the magnitude of the solution Eq. (18) is  $|\rho c| = 442$ .

This problem has been investigated in several publications [44, 27] and it has been shown that calculations with collocation BEM result in a decaying field along the duct, where the rate of decay depends on the frequency and the element size along the duct. As an example, the absolute value of the BEM solutions

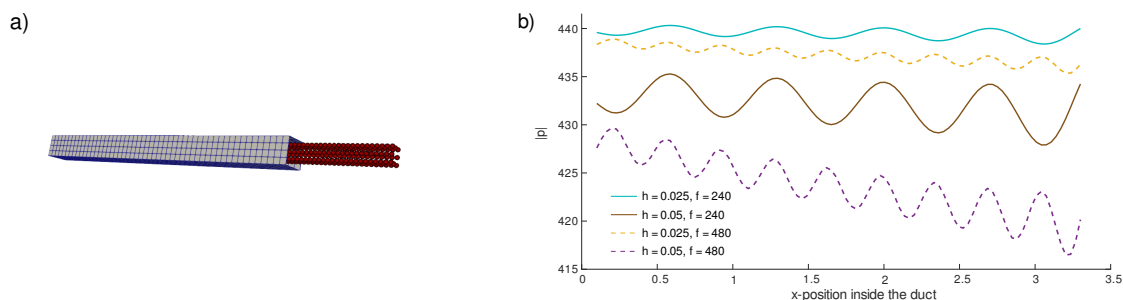


Figure 16: Discretization of the duct and the evaluation points inside the duct. Only parts of the duct surface are displayed. b) Magnitude in Pa of the pressure along a line inside the duct for different element sizes  $h$  at 240 Hz and at 480 Hz.

inside the duct for two different frequencies  $f_1 = 240$  Hz and  $f_2 = 480$  Hz, and two different discretizations with edge lengths  $h = 0.025$  m and  $h = 0.05$  m are presented in Fig. 16b. At these frequencies, a smooth and robust solution is expected. It can be easily seen, that the difference between the plane wave solution and the numerical solution grows along the length of the duct. Overall, the errors between calculated and analytic solutions are smaller than 6%. Nevertheless, this benchmark is one of the few problems, where the 6-to-8-elements-per-wavelength rule may not be enough to provide results that are accurate enough.

To better illustrate this fact, the boundary conditions at both ends at  $x = 0$  and  $x = L$  are changed to sound-hard conditions. For such a duct, the theoretical resonance frequencies<sup>2</sup> are at  $f = 50n$  Hz, with  $n \in \mathbb{N}$ . In Fig. 17 the specific frequency around 250 Hz where the acoustic field inside the duct has maximum energy is shown as a function of element size. It can be easily observed that the “resonance” frequency of the calculation is only close to the theoretical value if the edge length is about 0.1 m, which is way shorter than suggested by the 6-to-8-elements-per-wavelength rule. At 250 Hz, the wavelength is about  $\lambda = \frac{340}{250} \approx 1.36$  m,

<sup>2</sup>When neglecting the diameter of the duct.

which would require an edge length of an element of approximately  $h = 0.17$  m if 8 elements per wavelengths are assumed. In Fig. 17, the frequency with maximum energy for this element size is about 4 to 5 Hz away from the “correct” frequency.

A side note: In Fig. 17a, the frequency step size for the computation was 1 Hz. In the observed frequency range, the resonance is very sharp and in reality not at an integer frequency. Thus, the calculated acoustic field inside the duct is bounded, although it may become quite large. The values of 249 Hz are a bit misleading because of the frequency step size. If a finer frequency grid is used around 250 Hz (see Fig. 17b) we see that the calculated “resonances” are between 249.9 Hz and 250 Hz.

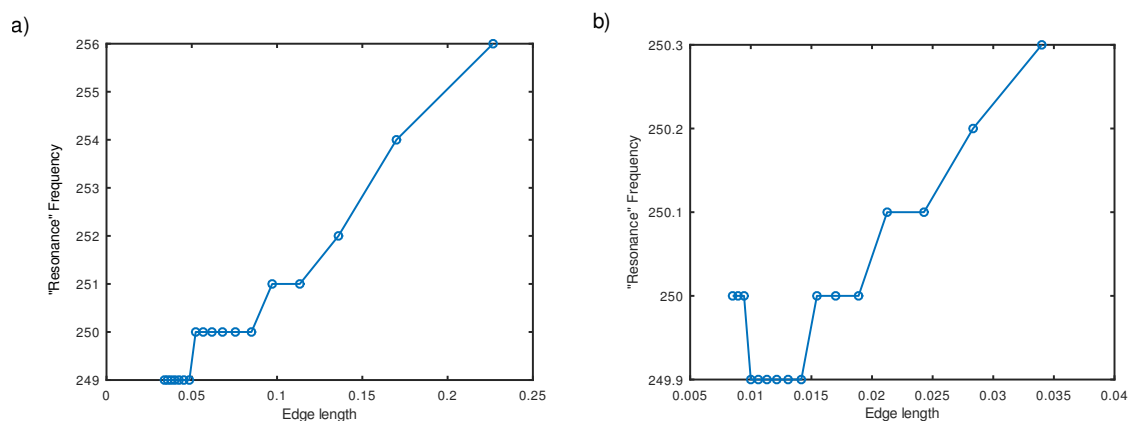


Figure 17: Frequencies at which the acoustic field inside the duct has maximum energy as a function of the element length  $\ell$  in the  $x$ -direction. The whole duct is assumed to be sound hard. The figure on the right side is a zoomed version of the figure on the left.

One explanation for the fact that 8 elements per wavelength are not enough to determine the “correct” resonance frequency, may be given by the fact, that, in theory, the field inside the duct is given by the combination of two plane waves travelling in opposite directions along the duct and that the zeros of the resulting standing wave at the resonance frequencies have to be resolved quite accurately.

## 6. Conclusion

In this paper, the open-source BEM program NumCalc, which is part of the open-source software project Mesh2HRTF, was described. The paper aims at a balance between giving researchers detailed information about certain aspects of the BEM implementation (Sections 3 and 5) and providing users with a general background of the BEM and the methods used in NumCalc (Sections 2, 4, and 5). The motivation behind the paper is to give users enough insight to decide if NumCalc is a good tool for their problem at hand.

An important aspect of NumCalc that users need to consider is that *NumCalc does not check the mesh before calculations*. In some cases, e.g., when elements contain double nodes or are twisted, there is a high

chance that the program will stop with an error message. However, in most cases, even when the normal vectors point in the wrong direction or the mesh contains holes, NumCalc will produce results, and *it is up to the user to check the validity of the results*. Throughout the paper, we provided general hints were added aiming at helping users to see if something goes wrong with the calculation. *”Do not use and trust any code blindly, check your results if they are plausible”*.

From experience and bugreports/requests, we encountered a few types of errors that are common. If users are “lucky”, the code stops with an error report, and users immediately see that there is a problem. The most common cause for such errors are badly shaped, loose or overlapping elements in the mesh. In Sec. 3.1, it was mentioned that if two elements are close together, one of them will be subdivided based on the distance of their midpoints. If elements are very irregular or even overlap, this distance criterion will never be fulfilled, thus the code stops after a fixed number of subdivisions. A second possible problem is that the iterative solver does not converge. One reason for that can also be a few distorted elements in the mesh, or some problems with the fast multipole method if the expansion length  $L$  gets too big, which is the case for a very large number of elements and if small and big elements are close together, i.e. if the mesh is locally not very regular.

In Section 3.3.1, we described the idea behind the expansion of the Green’s function and the problem with the truncation. If users encounter such a problem, one possible solution could be a change in the initial length of the boundary box in the FMM (see also Section 3.3). A second possible reason for problems with the stability is the direction of the normal vector, which somehow seems to be the most common error when using BEM. A wrong normal vector means that the role of interior problem and exterior problem is switched, which in turn means that in general sound sources are on the wrong side of the scatterer. If users are lucky, a wrong direction triggers some problem with the iterative solver, but in most of the cases, the code will finish without any problem, only the results will be, of course, completely wrong, which leads us the second type of error. In the “unlucky” case NumCalc runs without a problem, but the results do not make sense at all. Thus, the most important hint we can give is *”Check the plausibility of your results”*. It is easily possible that during a mesh reduction process loose vertices can get inserted, elements can get twisted, normal vectors can be inverted, holes can appear in the surface or external sound sources end up too close to the surface of the scatterer<sup>3</sup>. Technically, most of these irregularities are not really problems for the code itself, and such errors can only be discovered by checking the results of the computation.

In Sec. 5, a discussion about the accuracy and the memory requirements has been presented. It also provides users with a rough guideline on what to expect when using NumCalc, and it also should remind them on their responsibility to know if a numerical method or program is suitable to their problem at hand. In one of the examples it was shown that for low frequencies, it is possible that accuracy can suffer for fine

---

<sup>3</sup>Remember the Green’s function has a singularity at 0, so does the Hankel function used in the FMM.

grids. It was also shown, that this problems can be partly avoided by improving the accuracy of the code. But users should ask themselves, if it is really necessary to use such a fine grid for low frequencies in the first place. Sure, a coarser mesh, in general, means less accuracy, but is it necessary to invest computing time to achieve an accuracy of, e.g.,  $10^{-5}$  if other parameters like impedances or geometry have an uncertainty of about  $10^{-2}$ ?

Section 5 also showed that the estimation of the memory requirements of NumCalc is not always straightforward. To give a better estimation of the necessary memory, NumCalc has an additional option to just do a clustering, but no BEM computation, see [Appendix C.1](#). Based on the information about the size of the clusters a rough estimation of the necessary RAM can be given.

The head-and-torso example in [Sec. 5.2](#) also showed some of the limitations of NumCalc with respect to the needed RAM. As the length of the multipole expansion was high in the root level, the memory needed for storing the element-to-cluster matrices was relatively high. One way to prevent matrices with that many non-zero entries would be to restrict the size of the initial bounding box on the root level. This in turn results in clusters with smaller radii and therefore smaller expansion lengths  $L$ . As the number of non-zero entries of  $\mathbf{T}$  and  $\mathbf{S}$  depends on  $L$ , memory consumption can be reduced this way to some degree.

The discussion and examples provide a starting point for future improvements or adaptations to different computer architectures. If, for example, an architecture is used where memory is a bottleneck, e.g., GPUs, the memory consumption can be reduced by changing the clustering. But as it can be seen from the results for the example with head and torso, the memory consumption for large problems demand more sophisticated approaches than the ones currently used in NumCalc. NumCalc was originally aimed at midsize problems where the number of elements are between 60 000 and 120 000. Future developments will include dynamic clustering, interpolation and filtering between different multipole levels to avoid the storage of the matrices  $\mathbf{T}$  and  $\mathbf{S}$  at levels different from the leaf level, or different quadrature methods for the integrals over the unit sphere that are needed for the fast multipole method.

With respect to accuracy, we also plan on using methods to adapt the mesh size to the frequency used, which has the advantage of shorter computation times and an enhanced stability and accuracy in lower frequency bands. The simple example of plane wave scattering from a sound-hard sphere has already shown the general problem of having very fine grids at low frequencies. It is not a surprising fact that the condition of the scattering problem gets worse for fine meshes and low frequencies. This behavior can be motivated by the fact that the acoustic field at low frequencies changes only slightly, thus, the values on the collocation nodes are also almost the same, which has a negative influence on the stability of the system.

## Acknowledgements

We want to express our deepest thanks to Z.-S. Chen, who was the original programmer of the algorithms used in NumCalc and H. Ziegelwanger, who cleaned up the original code and created the original version of Mesh2HRTF.

This work was supported by the European Union (EU) within the project SONICOM (grant number: 101017743, RIA action of Horizon 2020).

## Appendix A. The Mesh

A mesh is a description of the geometry of scattering surfaces using *non-overlapping* triangles or plane quadrilaterals. The vertices of these elements are called BEM-nodes, their coordinates are defined via node lists that contain a unique node-number and the coordinates of each BEM-node in 3D (see Appendix [Appendix B.2](#)). The elements are provided using an element lists containing a unique element number and the node-numbers of the vertices for each element. These lists also provide information if the element lies on the surface of the scatterer (BEM-element) or away from the surface (evaluation elements, that are used, if users are also interested in the field around or inside the object) (see Appendix [Appendix B.2](#)). The unique normal vector of each element always needs to point away from the object, thus the vertices of each element should be ordered counterclockwise. The mesh should not contain any holes, each edge must be part of exactly two elements. The geometry described by the mesh should not contain parts that are very thin in relation to the element size, e.g. very thin plates or cracks, see also Sec. [4.1](#) and there should be at least 6 to 8 elements per wavelength, see also Sec. [5.1.2](#). The elements of the mesh should be as regular as possible. It improves the stability of the calculations, if elements are (at least locally) about the same size. Non-uniform sampling is possible as long as the change in element size is gradually, e.g., when using graded meshes towards singularities like edges or sudden changes in boundary conditions. In [\[25\]](#), a special kind of grading was developed, that used coarser grids away from regions with much detail, where even the 6-to-8-element rule was violated. This grading was possible because for the specific problem of calculating HRTFs, which was the application at hand, the geometry of the pinna of interest is much more important than the rest of the head. Nevertheless, it is up to the user to have a good look at the result of the computation to judge its quality.

A specific boundary condition needs to be assigned to each element of the mesh: Pressure, particle velocity normal to the element (see Appendix [Appendix B.3](#)), or (frequency dependent) admittance, see also Appendix [Appendix B.5](#). If no boundary condition is assigned to an element, it is automatically assumed to be sound hard, thus, the particle velocity is set to 0 and the element is acoustically fully reflecting. Admittance boundary conditions are used to model sound absorbing properties of different materials. On each element, it is possible, to combine an admittance boundary condition with a velocity

boundary condition. This additional velocity is used to model the effect of a vibrating part of the object, that generates sound.

## Appendix B. Example Input File

In the following, we present an example input file for the benchmark problem of a plane wave scattering from sound-hard sphere. We want to calculate the acoustic field for 10 frequencies between 100 and 1000 Hz, the plane wave moves along the  $z$  axis. The different parts of the input file will be described in the following subsections. A line in the input file that starts with the hash tag '#' is ignored by NumCalc and can be used for comments. The unit for the coordinates is meters, the speed of sound is given in m/s, and the density is given in  $\text{kg/m}^3$ .

```
Mesh2HRTF 1.0.0
Mesh for plane wave reflection on a sound hard sphere
##
## lines starting with '#' are ignored
##
##
## Controlparameters I, reserved for later use
##
0 0 0 0 7 0
##
## Controlparameter II: Frequency Steps
## (dummy, nSteps, stepsize, i0)
# do 10 frequency steps with stepsize 1 and start at s1 = i0 + stepsize
1 10 1.0 0.0
##
## Frequency Curve
#
# (Curvenr, Nr_of_Nodes)
0 2
# nodes of the piecewise linear curve
0.0 0
10.0 1000
## 1. Main Parameters I
## (nBGrps, nElems, nNodes, min. Explength, nLevelsSym,
```

```

## dummy, dummy, FMM_type, Solver)
## FMM_type = {0,1,4} = {No FMM, SLFMM, MLFMM}
## Solver = {0,4} = {CGS, direct Gauss Elimination}
2 28524 27042 8 0 2 1 4 0
##
## 2. Main Parameters II
# (nplanewaves, npointsracs, ext. vs. int. probl,
# default box length, default preconditioning)
1 0 0 0.0e0 0
##
## 3. Main Parameters III, not used (yet, anymore)
0 0 0 0
##
## 4. Main Parameters IV
## dSoundSpeed, dDensity, harmonic factor
3.400000e+02 1.300000e+00 1.000000e+00
#####
#
# Define the geometry of the mesh
#
#####
NODES
# Name of the file(s) containing the nodal data
TheBEMNodes.txt
TheEvalNodes.txt
ELEMENTS
# Name of the file(s) containing the nodal data
TheBEMElements.txt
TheEvalElems.txt
#####
#
# define the boundary conditions
# First Elem, Last Elem, Realpart, Curve, Imagpart, Curve
#

```

```

#####
BOUNDARY
# every element is sound hard, thus the default VELO = 0
# condition can be used, no input necessary
RETURN
#
# external sound sources
# planewave
# (Sourcenr, direction(x,y,z), realpart, curve, imagpart, curve
# pointsource
# (Sourcenr, source position (x,y,z), realpart, curve, imagpart, curve
#
PLANE WAVES
0 0.000000e+00 0.000000e+00 1.000000e+00 1.000000e+00 -1 0.000000e+00 -1
#
# if some frequency dependent admittance, or external sources are used,
# define the CURVES now
#
#CURVES
# no frequency dependent boundary conditions necessary
POST PROCESS
##
## BEM end of input ----
END
##
## this line seems to be important otherwise you end up in an
## endless loop, or at least add a return after END

```

Listing 1: Example input file for NumCalc

In the current version v1.1.1 of NumCalc, the input files needs to be named `NC.inp`.

### *Appendix B.1. Frequency-defining curves*

NumCalc numerically solves the Helmholtz equation in the frequency domain for a given set of frequencies defined by using frequency-defining curves. Frequency-defining curves are piece-wise linear functions that map a frequency step to a frequency or a frequency-dependent value of a boundary condition. The user

has to provide the nodes of these curves. An example: If one would want to calculate the sound field for 10 frequencies between 100 Hz and 1000 Hz in steps of 100 Hz, a simple way to describe the curve is given in Lst. 2. The first non-comment line consists of a dummy parameter (`dummy = 1`) followed by the number of frequency steps to be calculated (`nSteps = 10`) followed by the distance  $h_i$  between two frequency steps (`stepsize = 1.0`). The last entry in this line is given by the start index  $i_0$  of the curve (`i0 = 0.0`).

The next line contains the unique number of the curve (in case of a frequency definition, the curve number always needs to be `Curvenr = 0`) and the number of nodes defining the piece-wise linear function mapping the frequency step  $n$  to the respective frequency  $f_n$ . In Lst. 2, this map is defined as the line between the two nodes  $(S_1, F_1) = (0.0, 0.0 \text{ Hz})$  and  $(S_2, F_2) = (10.0, 1000.0 \text{ Hz})$ . The frequency for the  $n$ -th frequency step is then given as

$$f_n = F_1 + \frac{F_2 - F_1}{S_2 - S_1}((i_0 + h_i \cdot n - S_1) = 0 \text{ Hz} + \frac{1000 \text{ Hz}}{10}(0.0 + 1.0 \cdot n) = 100 \text{ Hz} \cdot n, n = 1, \dots, 10. \quad (\text{B.1})$$

```
## Controlparameter II: Frequency Steps
## (dummy, nSteps, stepsize, s0)
# do 10 frequency steps with stepsize 1 and start at s_1 = s0 + stepsize
1 10 1.0 0.0
##
## Frequency Curve
#
# (Curvenr, Nr_of_Nodes)
0 2
# nodes of the piece-wise linear curve
# (step, frequency)
0.0 0.0
10.0 1000.0
```

Listing 2: Definition of 10 uniform frequencies between 100 Hz and 1000 Hz

Also note that, for this example, the 6-to-8-elements-per-wavelength rule is *not* fulfilled for the two highest frequencies. Nevertheless, NumCalc will do the calculations, however, a warning will be displayed.

A more elaborate example is given in Lst. 3. This code snippet contains the definition of 8 third-octave frequency bands (see Fig. B.18), where three frequencies are chosen in each band.

### Appendix B.2. Nodes and Elements

The definition of the nodes (keyword `NODES`) and elements (keyword `ELEMENTS`) are done by providing the names of the text files containing the data for the nodes and the elements. There needs to be at least

```

#dummy n-steps stepsize
1      24  1.0 0.0
# Curvenr. Nr._of_Nodes
0      9
#define the curve
0.0  35.481
3.0  44.668
6.0  56.234
9.0  70.795
12.0 89.125
15.0 112.202
18.0 141.254
21.0 177.828
24.0 223.872

```

Listing 3: Definition of a frequency-defining curve for the third octave band example

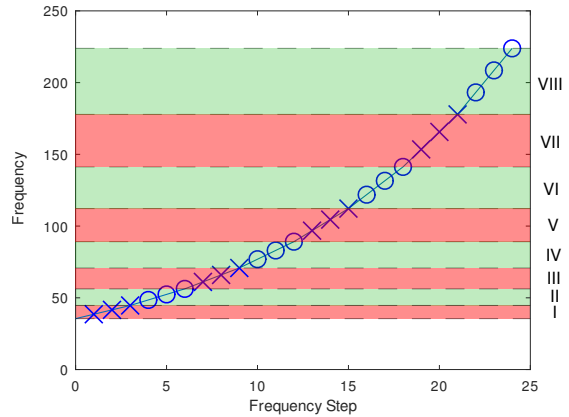


Figure B.18: Frequency-defining curve for the third octave band.

one file for the nodes and at least one file for the elements, but it is also possible to use more than one text file to describe different parts of the mesh. This has the advantage that the surface of the scatterer and an evaluation grid can be defined independently, as long as each node and each element have a unique identifying number. In the example input file Lst. 1 the information about the BEM nodes is given in the file `TheBEMNodes.txt`, whereas the coordinates of evaluation nodes not on the surface of the scatterer are given in `TheEvalNodes.txt`. The name of these files can be chosen arbitrarily by the user.

The structure of the node defining files is as follows: The first line needs to contain the number of nodes in the file, the following lines contain a unique node number, and the  $x, y, z$  coordinates of the node in meters. The first few lines in `TheBEMNodes.txt` looks for example like

```

2168
1 -5.773503e-01 -5.773503e-01 -5.773503e-01
2 -5.975550e-01 -5.975550e-01 -5.346551e-01
3 -6.174169e-01 -6.174169e-01 -4.874348e-01
...

```

Listing 4: First few lines of `TheBEMNodes.txt` containing the coordinates of the BEM nodes

Jumps in the node numbers are allowed, which makes it easier to mix surface meshes and evaluation points.

The definition of the element files is as follows: The first line again contains the number of elements in

the file. The next lines contain a unique integer to identify the element and the node numbers of the vertices of the element, followed by 3 integers. As an example, we show the first few lines of `TheBEMElements.txt` and `TheEvalElements.txt`

```
4332
1 381 382 458 0 0 0
2 381 458 457 0 0 0
3 382 383 459 0 0 0
...
```

Listing 5: First few lines of `TheBEMElements.txt` containing the definition of triangular surface elements

```
24192
5000 2169 2170 2351 2350 2 0 1
5001 2170 2171 2352 2351 2 0 1
5002 2171 2172 2353 2352 2 0 1
...
```

Listing 6: First few lines of `TheEvalElements.txt` containing the definition of the quadrilateral evaluation elements

The last three digits contain a flag for the type of elements, the number 0 and the group number of the element. NumCalc automatically determines from the number of the entries in each element line (7 or 8) if the element is triangular or quadrilateral (see Lst. 5 and 6). An element can either be a boundary element on the surface of an object (`type = 0`), or an element containing evaluation points (`type = 2`). Elements can also be assigned to different groups, but this feature is not recommended because the clustering for the FMM is done separately for each group. In general, it is sufficient to assign the BEM elements `GrpNr = 0` and evaluation elements `GrpNr = 1`.

### *Appendix B.3. Boundary conditions*

Boundary conditions describe the acoustic behavior of the scattering objects, the definition section starts with the keyword `BOUNDARY`. In NumCalc, three types of boundary conditions `{PRES,VELO,ADMI}` can be defined for each element. The general syntax for the boundary conditions is

```
ELEM e1 TO e2 bctype real(v0) curve1 imag(v0) curve2
```

This line means that all elements with element numbers in the interval `[e1, e2]` have the boundary condition `bctype`  $\in$  `{PRES,VELO,ADMI}` with value `v0`. With `PRES` the sound pressure can be fixed for the element, if the pressure is set to zero, the element is sound-soft. With `VELO` the particle velocity can be fixed for the given element, if the velocity is set to zero, the element is sound hard. With `ADMI` an admittance can be assigned to the element to model sound absorbing materials. In general, elements can only have one type

of boundary condition, however, it is possible, that elements can have an **ADMI** as well as a **VELO** boundary condition. This is done to model (vibrating) sound sources on sound-absorbing surfaces. If no condition is assigned to an element, it is automatically assumed to be sound hard.

As sound-absorbing behavior can be frequency dependent, **ADMI** conditions can be combined with a piece-wise linear curve (see Sec. [Appendix B.1](#)) that maps each frequency step to a scaling factor for the admittance. Thus, for the **ADMI** condition, **curve1** and **curve2** can contain the identifiers of piece-wise linear curves used to describe the frequency dependence of the real and imaginary part of the admittance. The curves are defined after the external sound source section. If no frequency dependence is needed, **curve1** and **curve2** are set to -1. The boundary condition section is closed using the keyword **RETURN**.

#### *Appendix B.4. Sound sources*

Besides vibrating sound sources on the scatterer, that are modelled by **VELO** boundary conditions, sources away from the surface can be given by a combination of point sources and plane waves.

A point source  $p_{\text{point}}(\mathbf{x}) := P_0 \frac{e^{ik\|\mathbf{x}-\mathbf{x}_0\|}}{4\pi\|\mathbf{x}-\mathbf{x}_0\|}$  at a source point  $\mathbf{x}_0$  is defined by its unique identifying number, the coordinates of its origin (**X0**,**Y0**,**Z0**) and its source strength **P0**:

**POINT**

Nr **X0 Y0 Z0 Real(P0) curve1 Imag(P0) curve2**

A plane wave  $p_{\text{planewave}}(\mathbf{x}) := P_0 e^{ik\mathbf{d}\cdot\mathbf{x}}$ ,  $\|\mathbf{d}\| = 1$  with direction (**DX**,**DY**,**DZ**) and strength **P0** is given by

**PLANE**

Nr **DX DY DZ Real(P0) curve1 Imag(P0) curve2**

If the input is not dependent on the frequency, the curves identifiers are **curve1 = curve2 = -1**.

#### *Appendix B.5. Frequency definition curves for admittance*

If an admittance boundary condition or the strength of the external sound sources need to be frequency dependent, it is necessary to define additional scaling curves dependent on the frequency steps. The definition of the curves begins with the keyword **CURVES** followed by a line containing the **number\_of\_curves** and the largest number of nodes **nMaxCurves** that define these curves. Each single curve is then defined by one line containing the unique curve number **icurve** and the number of nodes **inodes** defining the respective curve. The next **inodes** lines contain the nodes of the piece-wise linear curve similar to the frequency definition curve. An example:

**CURVES**

# **number\_of\_curves max\_number\_of\_points\_per\_curve**

2 4

```

# curve_number  number_of_nodes_defining_curve
1 4
0.0 0.0
1.0 1.0
3.0 4.0
8.0 6.0
# curve_number  number_of_nodes_defining_curve
2 3
0.0 0.0
2.0 2.0
10.0 9.0

```

defines two curves (one for the realpart, one for the imaginary part) that are used to define a frequency dependent admittance `ELEM e0 TO e1 ADMI real(v0) 1 imag(v0) 2`, which assigns all elements between `e0` and `e1` a frequency dependent admittance  $\alpha(s) = c_1(s) \text{real}(v0) + ic_2(s) \text{imag}(v0)$  with

$$c_1(s) = \begin{cases} s & \text{for } s \in [0, 1], \\ 1 + \frac{3}{2}(s - 1) & \text{for } s \in [1, 3], \\ 4 + \frac{2}{5}(s - 3) & \text{for } s \in [3, 8], \end{cases}$$

and

$$c_2(s) = \begin{cases} s & \text{for } s \in [0, 2], \\ 2 + \frac{7}{8}(s - 2) & \text{for } s \in [2, 10]. \end{cases}$$

The frequency steps  $s$  have already been defined via the frequency definition curve, e.g., the curve defined in Section [Appendix B.1](#).

## Appendix C. Command-line options

Besides the parameter option that can be set using the input file `NC.inp`, there is the additional option start NumCalc with command line parameters.

### Appendix C.1. Estimation of memory consumption

The discussion about the non-zero entries of the multipole matrices in Secs. [3.3.5](#) and [3.3.6](#) has also shown that the clustering is very dependent on the mesh and that the numbers of clusters in the nearfield and the interaction list can vary to a large degree. As it is hard to estimate beforehand how the clustering will look like exactly, NumCalc provides users with the option to just compute the clustering and the number of non-zero entries of the FMM matrices *without* doing actual BEM calculations. If users start NumCalc

with `NumCalc --estimate_ram` an estimation of the memory needed based on the entries of the multipole matrices is done. However, auxiliary variables and arrays to store mesh data and results are neglected in this estimation. Thus, the estimate slightly underestimates the RAM needs. For the example of the sphere, `NumCalc` estimates the necessary RAM to be 0.095 GByte, whereas `Gnu/time` [45] listed the maximum memory consumption with 0.116 GByte. This difference can be explained partly by the number  $N_e = 24884$  of evaluation nodes used in this example. If  $N_e = 70$  the memory consumption is reduced to about 0.1 GByte. Nevertheless, this feature helps to get a rough idea to reserve the right amount of memory for calculations on a computer cluster.

### *Appendix C.2. Parallelization*

As the BEM systems for different frequencies are independent of each other, parallelization is straight forward. `NumCalc` offers users the option to use the same input file for different ranges of frequency-steps. If, for example, only the first 10 frequencies should be calculated using one single thread, `NumCalc` can be started using `NumCalc -istart 1 -iend 10`, whereas a second thread can handle the next 10 frequencies using `NumCalc -istart 11 -iend 20`. However, it is up to the user to distribute the jobs over the different nodes of a computer cluster.

## **Appendix D. Output**

The output of `NumCalc` can be split into two file types. First, there is `NC.out`<sup>4</sup> containing general information, e.g., frequencies used, information about the mesh, the highest frequency where the 6-to-8-elements-per-wavelength rule is still valid and similar data. This file also contains information about the FMM, e.g., the number of clusters and the expansion lengths for each level, and information about the number of iterations and the final error of the iterative solver.

Second, the results of the calculations are stored in the folder `be.out`. This folder contains several sub-folders `be.n`, one for each frequency step  $n$ . Inside each of these folders, one can find the files

- `pBoundary` containing the real and imaginary part of the sound pressure at the midpoints of each element,
- `vBoundary` containing the real and imaginary part of the particle velocity normal to the surface at the midpoints of each element,
- `pEvalGrid` containing the real and imaginary part of the sound pressure at each evaluation point,
- `vEvalGrid` containing the real and imaginary part of the particle velocity in the  $x$ ,  $y$ , and  $z$  direction.

---

<sup>4</sup>Or `NC{step1}-{step2}.out` if the command line parameters `-istart` and `-iend` are used.

The structure of having separate folders for each frequency step has the advantage that the calculation for different frequency steps can be easier distributed on different nodes of a computer cluster.

## References

- [1] Z.-S. Chen, H. Waubke, W. Kreuzer, A Formulation of the Fast Multipole Boundary Element Method (FMBEM) for Acoustic Radiation and Scattering from Three-dimensional Structures, *J. Comput. Acoust.* 16 (2) (2008) 303–320.
- [2] S. Sauter, C. Schwab, *Boundary Element Methods*, Springer Series in Computational Mathematics, Springer Berlin Heidelberg, 2010.
- [3] S. Marburg, B. Nolte (Eds.), *Computational Acoustics of Noise Propagation in Fluids - Finite and Boundary Element Methods*, Springer, Berlin, 2008, Ch. PART II FEM: External Problems, pp. 35–250.
- [4] R. Coifman, V. Rokhlin, S. Wandzura, The fast multipole method for the wave equation: A pedestrian prescription, *IEEE Trans. Antennas Propag.* 35 (3) (1993) 7–12.
- [5] V. Rokhlin, Rapid solution of integral equations of scattering theory in two dimensions, *J. Comput. Phys.* 86 (2) (1990) 414–439.
- [6] V. Rokhlin, Diagonal forms of translation operators for the Helmholtz equation in three dimensions, *Appl. Comput. Harmon. Anal.* 1 (December 1993) 82–93.
- [7] W. Hackbusch, *Hierarchical Matrices: Algorithms and Analysis*, Springer, 2015.
- [8] COMSOL Inc., COMSOL, <http://www.comsol.com> (accessed 06.09.2023).
- [9] FastBEM, FastBEM, <https://fastbem.com>, (accessed 2022-05-13).
- [10] U. Iemma, V. Marchese, AcouSTO, <http://acousto.sourceforge.io>, (accessed 2022-05-13).
- [11] T. Betcke, M. Scroogs, Bempp-cl: A fast Python based just-in-time compiling boundary element library., *J. Open Source Softw.* 6 (59) (2021) 2879. doi:10.21105/joss.02879.
- [12] V. Henriquez, J. Møller, OpenBEM - an open source boundary element method software in acoustics, in: INTERNOISE 2010 - 39th International Congress on Noise Control Engineering 2010, Lisbon, Portugal, 2010.
- [13] W. Kreuzer, K. Pollack, P. Majdak, F. Brinkmann, Mesh2HRTF/Numcalc: An Open-Source Project to Calculate HRTFs and wave scattering in 3D, in: BNAM2022, Aalborg, 2022.
- [14] F. Brinkmann, W. Kreuzer, J. Thomsen, S. Dombrovskis, K. Pollack, S. Weinzierl, P. Majdak, Recent Advances in an Open Software for Numerical HRTF Calculation, *J. Audio Eng. Soc.* 71 (7/8) (2023) 502–514. doi:10.17743/jaes.2022.0078.
- [15] The Mesh2HRTF Developers, Mesh2HRTF – An open source software for the numerical calculation of head-related transfer functions, <https://mesh2hrtf.org>, (accessed 2022-12-20).
- [16] H. Ziegelwanger, W. Kreuzer, P. Majdak, Mesh2HRTF: An open-source software package for the numerical calculation of head-related transfer functions, in: *Proceeding of the 22nd International Congress on Sound and Vibration*, Florence, Italy, 2015. doi:10.13140/RG.2.1.1707.1128.
- [17] H. Møller, M. F. Sørensen, D. Hammershøi, C. B. Jensen, Head-related transfer functions of human subjects, *J Audio Eng. Soc.* 43 (1995) 300–321.
- [18] P. Majdak, P. Balazs, B. Laback, Multiple exponential sweep method for fast measurement of head-related transfer functions, *J Audio Eng Soc* 55 (2007) 623–637.
- [19] K. Pollack, W. Kreuzer, P. Majdak, Perspective chapter: Modern acquisition of personalised head-related transfer functions – an overview, in: *Advances in Fundamental and Applied Research on Spatial Audio*, IntechOpen, 2022. doi:10.5772/intechopen.102908.
- [20] Blender Online Community, Blender 3.6 reference manual, <https://docs.blender.org/manual/en/latest/index.html> (accessed 06.09.2023).

- [21] The Mesh2HRTF Developers, Mesh2HRTF Wiki, <https://github.com/Any2HRTF/Mesh2HRTF/wiki>, (accessed 2022-12-20).
- [22] A. J. Burton, G. F. Miller, The application of integral equation methods to the solution of exterior boundary-value problems, *Proc. R. Soc. London Ser. A* 323 (1971) 201–210.
- [23] H. A. Schenck, Improved integral formulation for acoustic radiation problems, *J. Acoust. Soc. Am.* 44 (1) (1968) 41–58.
- [24] S. Marburg, Six boundary elements per wavelength. Is that enough?, *J. Comput. Acoust.* 10 (2002) 25–51. doi:10.1142/S0218396X02001401.
- [25] H. Ziegelwanger, W. Kreuzer, P. Majdak, A priori mesh grading for the numerical calculation of the head-related transfer functions, *Appl. Acoust.* 114 (2016) 99–110. doi:https://doi.org/10.1016/j.apacoust.2016.07.005.
- [26] T. Palm, S. Koch, F. Brinkmann, M. Alexa, Curvature-adaptive mesh grading for numerical approximation of head-related transfer functions, in: *Fortschritte der Akustik – DAGA 2021*, Vienna, Austria, 2021, pp. 1111–1114.
- [27] W. Kreuzer, Numerical simulation of sound propagation in and around ducts using thin boundary elements, *J. Sound Vibr.* 534 (2022) 117050. doi:https://doi.org/10.1016/j.jsv.2022.117050.
- [28] S. Marburg, A review of the coupling parameter of the Burton and Miller boundary element method, in: *INTERNOISE 2014 - 43rd International Congress on Noise Control Engineering: Improving the World Through Noise Control*, 2014.
- [29] E. Anderson, Z. Bai, C. Bischof, S. Blackford, J. Demmel, J. Dongarra, J. Du Croz, A. Greenbaum, S. Hammarling, A. McKenney, D. Sorensen, *LAPACK Users' Guide*, 3rd Edition, Society for Industrial and Applied Mathematics, Philadelphia, PA, 1999.
- [30] Y. Saad, *Iterative Methods for Sparse Linear Systems*, 2nd Edition, Society for Industrial and Applied Mathematics, 2003. doi:10.1137/1.9780898718003.
- [31] M. Duffy, Quadrature over a pyramid or cube of integrands with a singularity at a vertex, *SIAM J. Numer. Anal.* 19 (6) (1982) 1260–1262.
- [32] G. Krishnasamy, L. Schmerr, T. Rudolphi, F. Rizzo, Hypersingular boundary integral equations: Some applications in acoustic and elastic wave scattering, *J. Appl. Mech.* 57 (1990) 404–414.
- [33] J. Lachat, J. Watson, Effective numerical treatment of boundary integral equations: A formulation for three-dimensional elastostatics, *Int. J. Numer. Methods Eng.* 10 (1976) 991–1005.
- [34] M. Abramowitz, I. Stegun, *Handbook of Mathematical Functions with Formulas, Graphs, and Mathematical Tables*, Dover, New York, 1964.
- [35] G. Cowper, Gaussian quadrature for triangles, *Num. Meth. Eng.* 7 (3) (1973) 405–408.
- [36] K.-J. Bathe, *Finite-Elemente-Methoden (Finite Element Methods)*, 2. Auflage, Springer, Berlin, Heidelberg, New York, Barcelona, Hongkong, London, Mailand, Paris, Tokio, 2014.
- [37] A. Meister, *Numerik linearer Gleichungssysteme*, Vieweg & Sohn Verlagsgesellschaft GmbH, Braunschweig/Wiesbaden, 1999.
- [38] J. Rahola, Diagonal forms of the translation operators in the fast multipole algorithm for scattering problems, *BIT* 36 (2) (1996) 333–358.
- [39] C. Cecka, E. Darve, Fourier based fast multipole method for the Helmholtz equation, *SIAM J. Sci. Comput.* 35 (1) (2013) A79–A103.
- [40] S. Amini, A. Profit, Multi-level fast multipole solution of the scattering problem, *Eng. Anal. Bound. Elem.* 27 (2003) 547–564.
- [41] K. Giebermann, *Schnelle Summationsverfahren zur numerischen Lösung von Integralgleichungen für Streuprobleme im  $\mathbb{R}^3$*  (Fast summation methods for the numerical solution of integral equations for scattering problems in  $\mathbb{R}^3$ ), Ph.D. thesis, Universität Karlsruhe (1997).
- [42] E. G. Williams, *Fourier Acoustics. Sound Radiation and Nearfield Acoustical Holography*, Academic Press, San Diego, London, Boston, New York, Sydney, Tokyo, Toronto, 1999.

- [43] M. Hornikx, M. Kaltenbacher, S. Marburg, A platform for benchmark cases in computational acoustics, *Acta Acust. united Ac.* 101 (2015) 811–820.
- [44] S. Marburg, A pollution effect in the boundary element method for acoustic problems, *J. Theor. Comput. Acoust.* 26 (2) (2018) 1850018.
- [45] A. Gordon, Gnu Time, <https://www.gnu.org/software/time/> (last visited 26.07.2022).